Petrogenesis and tectonic setting of a granitic pluton in the northern Ya-Gan fault zone, North Alxa, China: Constraints from whole-rock geochemistry, zircon U–Pb ages, and Sr–Nd–Hf isotope compositions

Fenquan Xie [1,2,3], Qianhong Wu[1,2]*, Lidong Wang[4]*, Zhaoxia Shi[5]
Wenzhou Xiao[1,2], Jingya Cao[1,2], Biao Liu[1,2], Jiangbo Jiang [1,2], Jiajia Song [4]

Corresponding authors: Qianhong Wu xfqyongyuan@csu.edu.cn
Lidong Wang xfqyongyuan@yeah.net

1. School of Geosciences and Info-Physics, Central South University, Changsha 410083, China
2. Key Laboratory of Metallogenic Prediction of Nonferrous Metals and Geological Environment Monitoring Ministry of Education, Changsha 410083, China
3. Eighth Geological Brigade of Hebei Bureau of Geology and Mineral Resources Exploration, Qinhuangdao 066001, China
4. The School of Water Resource and Environment, China University of Geosciences Beijing 100083,China
5. Office of Academic Affairs, Yanshan University, Qinhuangdao 066004,China

ABSTRACT: A series of precise data consisting of zircon U–Pb ages, whole-rock geochemistry and Sr–Nd–Hf isotope compositions from the Huhetaoergai granitic pluton was collected in this study and combined with data from the western Huhetaoergai, Zhuxiaogubuhe and Yagan granitic plutons to constrain the petrogenesis and tectonic setting of granitic plutons in the northern Ya-Gan fault zone, North Alxa, China. The Huhetaoergai pluton is composed of hornblende diorite, medium- to coarse-grained biotite adamellite and coarse-grained biotite adamellite

 doi:10.20944/preprints201806.0344.v1

with K-feldspar megacrysts. The U–Pb zircon ages of biotite adamellite are 220.5 ± 1.9 Ma and 226.5 ± 2.4 Ma. These granitoids are I-type granites with highly radiogenic initial $^{87}Sr/^{86}Sr$ of 0.708085–0.735470, negative εNd(t) average values of -2.98–3.23 and high εHf(t) of 9–11.05. These features indicate the granitoids were formed from magmas generated from juvenile crust. We speculate that the granitoids of the Huhetaoergai pluton were emplaced during an episode of intense intraplate orogenic movement evolution in an extrusional setting after a period of extensional postcollisional intraplate evolution.

Keywords: Huhetaoergai pluton; Yagan Belt; I-type granites; Geochemistry; Zircon U–Pb dating; Sr–Nd–Hf isotopes.

1. Introduction

The Central Asia Orogenic Belt (CAOB), also called the “Central Asian mobile belt”, “Central Asian Fold belt” or “Altaids”, is one of the largest accretionary orogens on Earth and one of the most important areas for the growth of continental shells, situated at the suture of the European, Siberian, Tarim, and Sino-Korean cratons (Fig. 1a). The northern margin of the Alxa block is located in the middle of the southern margin of the CAOB and is in the key position connecting the structural units on both sides of the CAOB; then, it is an important area to study the final closure process of the Paleo-Asian Ocean.

Previous studies have been focused on the division of the Alxa block and the stratigraphic evolution of the Precambrian in the northern margin of the Alxa block

 doi:10.20944/preprints201806.0344.v1

However, few studies have been conducted in the northern region of the Alxa block and in Mongolia.

The northern margin of the Alxa block is covered by the Badain Jaran Desert, and because of the formidable natural conditions, geological research is relatively scarce. Since the 1980s, some scholars have systematically studied the Paleozoic crustal evolution in the northern margin of the Alxa block, made a preliminary division of the tectonic units in this area, and established the basic pattern of tectonic evolution, which established a good foundation for future research work.

Due to the long-term interactions between different plates, the regional geologic setting of the Alxa block is extremely complex. The Alxa block is mainly composed of ophiolitic mélanges, island arcs, oceanic basins, trenches and continental margins, and three fault zones occur in this block, which are from north to south the Ya-Gan fault, Engger Us Ophiolite Belt, and Qagan Qulu Ophiolite Belt (Fig. 1b) [3-5]. The existing studies have researched the area north of the Engel Wusu fault zone as a whole, but there is no detailed study of the structural properties of the Ya-Gan tectonic belt, which is of great importance [3]. The Ya-Gan fault zone can be connected to the Mingshui-Xiaoxingshan ophiolite zone in the west, and a former study suggested that the Mingshui-Xiaoxingshan ophiolite zone is a stitching zone between the Kazakhstan plate and the Tarim plate [6]. However, there is no clear evidence about the closure time and the tectonic evolution during the Paleozoic between the Kazakhstan and the Tarim plates in the northern Alxa area because an ophiolitic mélange associated with the collision of the Tarim and Kazakhstan plates has not yet been found in the Ya-Gan

 doi:10.20944/preprints201806.0344.v1

fault zone.

The Huhetaoergai pluton is located on the north side of the Ya-Gan fault zone and has an area of approximately 80 km^2, one of the plutons with widespread exposure in the northern area of Alxa. In this paper, we present new data from laser ablation inductively coupled plasma mass spectrometry (LA-ICP-MS) zircon U–Pb dating and analysis of trace element contents, whole-rock geochemistry, and Sr–Nd–Hf isotopes in samples from the Huhetaoergai pluton, combined with data collected from the Zhuxiaogubuhe pluton, western Huhetaoergai pluton, and Yagan pluton, with the aims of (1) outlining the petrogenesis of the pluton; (2) constraining the source and origin of the granitic magmas; and (3) discussing the tectonic setting of the pluton.

2. Geological background

The Huhetaoergai pluton is located northeast of Ejinaqi, occupies an area of ~80 km^2 and consists of many intrusive rocks that are intruded into Paleozoic rocks dominated by Ordovician strata (Fig. 1c). The circular Huhetaoergai pluton has sharp contacts with the surrounding rocks at inclinations of 45°~70°. In the vicinity of the contact surface, the interpenetration of apophyses is common, and assimilation and contamination are stronger where we can see xenoliths. The thermal deterioration of the surrounding rock is strong, forming a contact metamorphic belt with a width of several hundred meters [7].

The granitoids within the Huhetaoergai pluton are typically massive, leucocratic

 doi:10.20944/preprints201806.0344.v1

and porphyritic and can be subdivided into two rock types: medium- to coarse-grained biotite adamellite and coarse-grained biotite adamellite with K-feldspar megacrysts. The xenoliths are hornblende diorite and are composed of quartz (~5%), plagioclase (~50%), amphibole (~40%), and biotite (~5%) (Fig. 2a, b).The medium- to coarse-grained biotite adamellite is composed of quartz (~35%), K-feldspar (~30%), plagioclase (~25%), and biotite (~10%) with accessory zircon, apatite, and magnetite (Fig. 2c, d). The coarse-grained biotite adamellite with K-feldspar megacrysts consists of quartz (~20%), K-feldspar (~40%), plagioclase (~25%), and biotite (~15%) with accessory zircon, apatite, sphene, and magnetite (Fig. 2e, f).

Eleven samples were collected from the granitoids of the Huhetaoergai pluton. Samples Ch03 and Ch06 were collected from the Hornblende diorite in the Xenoliths. Samples Ch01, Ch02, Ch04, Ch07, Ch08, Yh22, and Yt21 were collected from the medium- to coarse-grained biotite adamellite, which are similar in texture to the Indosinian granitoids in the study area. Samples Ch05 and Yt20 were collected from the coarse-grained biotite adamellite with K-feldspar megacrysts.

3. Samples and analytical techniques

3.1. Zircon U–Pb dating

Two samples (Ch08 and Yh22) were selected for zircon U–Pb dating. Zircon grains from these samples were separated by conventional magnetic and heavy liquid techniques before they were hand-picked under a binocular microscope. They were

 doi:10.20944/preprints201806.0344.v1

then mounted into epoxy resin blocks and polished to obtain flat surfaces. The preparations were conducted by Langfang Geoscience Exploration Technology Services Co. Ltd., China.

U–Pb dating analyses were conducted by laser ablation multicollector inductively coupled plasma mass spectrometry (LA-MC-ICP-MS) at the Institute of Mineral Resources, Chinese Academy of Geological Sciences, Beijing. Detailed operating conditions for the laser ablation system and the MC-ICP-MS instrument and data reduction were the same as described by [8]. Laser sampling was performed using a Newwave UP 213 laser ablation system. A Thermo Finnigan Neptune MC-ICP-MS instrument was used to acquire ion-signal intensities. The array of four multi-ion-counters and three faraday cups allowed simultaneous detection of 202Hg (on IC5), 204Hg, 204Pb (on IC4), 206Pb (on IC3), 207Pb (on IC2), 208Pb (on L4), 232Th (on H2), and 238U (on H4) ion signals. Helium was applied as the carrier gas. Argon was used as the make-up gas and mixed with the carrier gas via a T-connector before entering the ICP. Each analysis incorporated a background acquisition of approximately 20-30 s (gas blank) followed by 30 s of data acquisition from the sample. Off-line raw data selection, integration of background and analyte signals, time-drift correction and quantitative calibration for U-Pb dating were performed by ICP-MS-DataCal [9].

Zircon GJ1 was used as an external standard for U–Pb dating and was analyzed twice every 5-10 analyses. Time-dependent drifts of U–Th–Pb isotopic ratios were corrected using linear interpolation (with time) for every 5-10 analyses according to

Preprints (www.preprints.org) | NOT PEER-REVIEWED | Posted: 22 June 2018 doi:10.20944/preprints201806.0344.v1

the variations in GJ1 (i.e., 2 zircon GJ1 + 5-10 samples + 2 zircon GJ1)[9]. The preferred U–Th–Pb isotopic ratios used for GJ1 were from Jackson et al. (2004). The uncertainty of preferred values for the external standard GJ1 was propagated to the ultimate results for the samples. In all analyzed zircon grains, the common Pb correction was not necessary due to the low signal of common 204Pb and high 206Pb/204Pb. U, Th and Pb concentrations were calibrated by zircon M127 (with U: 923 ppm; Th: 439 ppm; Th/U: 0.475) [10] . Concordia diagrams and weighted mean calculations were made using Isoplot/Ex_ver3. The zircon Plesovice was dated as an unknown sample and yielded a weighted mean 206Pb/238U age of 337 ± 2 Ma (2 SD, n = 12), which was in good agreement with the recommended 206Pb/238U age of 337.13 ± 0.37 Ma (2 SD) [11].

3.2. Whole-rock major and trace element analysis

Whole-rock major and trace element compositions were analyzed at the Analytical Laboratory of the Beijing Research Institute of Uranium Geology, China. The samples were crushed in a milling machine to pass 200 mesh before major element contents were measured using an AB-104 L and PW2404 X-ray fluorescence (XRF) instrument with an analytical accuracy of approximately 1–5%. Trace element compositions were measured using ICP-MS (an ELEMENT XR 9443 instrument) with an analytical accuracy of better than 5%.

 doi:10.20944/preprints201806.0344.v1

3.3. Sr–Nd isotope composition analysis

Prior to isotope analysis, the samples were crushed in a milling machine to pass 200 mesh. Sr–Nd isotope compositions were measured using multicollector thermal ionization mass spectrometer (MC-TIMS) housed at Langfang Geoscience Exploration Technology Services Co. Ltd. Hebei Province, China. Rb and Sr were separated and purified using conventional cation exchange, whereas Sm and Nd were separated and purified using Teflon and a Power resin, respectively. The Sr–Nd isotope ratio correction for mass fractionation was undertaken by normalizing to $^{86}Sr/^{88}Sr = 0.1194$ and $^{146}Nd/^{144}Nd = 0.7219$. The $^{87}Sr/^{86}Sr$ ratio of the Sr standard (NBS987) and the $^{143}Nd/^{144}Nd$ ratio of the Nd standard (La Jolla) used in this study were 0.710249 ± 0.000012 (2σ) and 0.511869 ± 0.000006 (2s), respectively. The analytical accuracy of the Sr and Nd isotope data were better than 0.003%. Specific procedures for the isotope analytical techniques are given by Chen et al. (2002) [12].

3.4. Lu–Hf isotope composition analysis

Zircon Hf isotope analysis was carried out in situ using an ESI NWR193 laser ablation microprobe attached to a Neptune Plus Multicollector ICP-MS at Beijing CreaTech Testing International Co., Ltd., Beijing. Instrumental conditions and data acquisition were comprehensively described by Wu et al. (2006) [13] and Hou et al. (2007) [14]. A stationary spot was used for the present analyses, with a beam diameter of 40 μm depending on the size of ablated domains. Helium was used as the carrier gas to transport the ablated sample from the laser ablation cell to the ICP-MS torch

Preprints (www.preprints.org) | NOT PEER-REVIEWED | Posted: 22 June 2018 doi:10.20944/preprints201806.0344.v1

via a mixing chamber mixed with argon. To correct the isobaric interferences of 176Lu and 176Yb on 176Hf, 176Lu/175Lu = 0.02658 and 176Yb/173Yb = 0.796218 ratios were determined [15]. For instrumental mass bias correction, Yb isotope ratios were normalized to a 172Yb/173Yb ratio of 1.35274 [15] and Hf isotope ratios to a 179Hf/177Hf ratio of 0.7325 using an exponential law. The mass bias behavior of Lu was assumed to follow that of Yb, and the mass bias correction protocol details were described by Wu et al. (2006) [13] and Hou et al. (2007)[14]. Zircon GJ1 was used as the reference standard during our routine analyses with a weighted mean 176Hf/177Hf ratio of 0.282007 ± 0.000007 (2σ, n = 36). This value is not distinguishable from a weighted mean 176Hf/177Hf ratio of 0.282000 ± 0.000005 (2σ) using the solution analysis method by Morel et al. (2008) [16].

4. Analytical results

4.1 Zircon U–Pb dating results

Zircons crystals from samples Ch08 and Yh22 are mainly euhedral and colorless or light yellow, and the morphologies of zircons are mainly granular and columnar; zircons have a high degree of crystallinity and exhibit the characteristics of magmatic zircons. Additionally, the samples have high Th/U ratios (between 0.41 and 1.31), which are consistent with a magmatic genesis [17-18].

Zircon crystals from sample Ch08 are typically euhedral with lengths ranging from 150 to 300 μm and length-to-width ratios ranging from 1:1 to 3:1.

Preprints (www.preprints.org) | NOT PEER-REVIEWED | Posted: 22 June 2018 doi:10.20944/preprints201806.0344.v1

Cathodoluminescence (CL) imaging indicates the clear, rhythmic and bright and dark ring structure, and most of the zircon grains have internal oscillatory zoning that is typical of magmatic origin [19] Fig. 3a). The $^{206}Pb/^{238}U$ ages of 15 zircon grains from this sample range from 218.7 to 223.9 Ma (Table 1) and plot on or close to the concordia curve with a weighted mean $^{206}Pb/^{238}U$ age of 220.5 ± 1.9 Ma (MSWD = 2.9; Fig. 3b).

Zircon crystals from sample Yh22 are mostly euhedral and much smaller than those from sample Ch08 with lengths ranging from 200 to 450 μm and length-to-width ratios ranging from 1:1 to 5:1 (Fig. 3c). Most of these zircon crystals display oscillatory zoning. Analysis of 19 zircon grains from this sample yielded $^{206}Pb/^{238}U$ ages ranging from 221 to 228 Ma (Table 1) and a weighted mean $^{206}Pb/^{238}U$ age of 226.5 ± 2.4 Ma (MSWD = 0.19; Fig. 3d).

4.2 Whole-rock major and trace element geochemistry

The analytical results for whole-rock major and trace elements in the samples taken from the granitoids in the Huhetaoergai pluton are shown in Table 2. Previously published data [20-21] are also cited and discussed in this study. The samples Ch01, Ch02, Ch04, Ch05, Ch07, Ch08, Yh22, Yt-20, and Yt-21 have relatively wide ranges in chemical compositions with SiO_2 = 64.68–76.61%, TiO_2 = 0.05–0.79%, Al_2O_3 = 13.23–16.51%, TFe_2O_3 = 0.76–7.18%, MgO = 0.13–1.85%, K_2O = 2.95–4.47%, and P_2O_5 = 0.01–0.29%. All samples have high total alkali contents (K_2O+Na_2O = 6.69–8.33%). The values of TiO_2, Al_2O_3, TFe_2O_3, MgO, CaO, Na_2O, P_2O_5, and K_2O are negatively related to SiO_2 (Fig. 4), and the rocks are classified in the high-K calc-alkaline series (Fig. 4i). All of the studied samples plot in the "subalkalic granites" field on the (K_2O+Na_2O) vs. SiO_2 diagram (Fig. 5a). Samples Ch03 and

Preprints (www.preprints.org) | NOT PEER-REVIEWED | Posted: 22 June 2018 doi:10.20944/preprints201806.0344.v1

Ch06 are diorites, and the other samples are granodiorite-granite. The granite A/CNK (molar $Al_2O_3/[CaO + Na_2O + K_2O]$) values range from 0.94 to 1.25, and their A/NK (molar $Al_2O_3/[Na_2O + K_2O]$) values range from 1.18 to 1.60. All samples plot in the metaluminous and peraluminous areas on the A/CNK vs. A/NK diagram (Fig. 5b). The rocks have moderate alkali contents with all data plotting in the calc-alkaline field (Fig. 5c). Some rocks are fall into the pure crustal partial melts feild and some show higher $Mg^{\#} = Mg/(Mg+FeT)$ than pure crustal partial melts (Fig. 5d).

All granitoid samples in the Huhetaoergai pluton show similar chondrite-normalized rare earth element (REE) patterns that are characterized by enrichment in light REEs (LREEs) with high $(La/Yb)_N$ ratios (1.49–41.69) and weakly negative Eu anomalies (Eu/Eu* = 0.41–0.85; Fig. 6a). These samples also show similar primitive-mantle-normalized trace element patterns characterized by enrichment in large ion lithophile elements (LILE, e.g., Rb, K, U, and Th) and depletion in high field strength elements (HFSE, e.g., Ti, P, Sr, Ba, and Nb; Fig. 6b). The chondrite-normalized REE patterns and primitive mantle-normalized trace element patterns of the diorites such as samples Ch03 and Ch06 are similar to those of the granitoids. The heavy and medium REEs (HREEs and MREEs) in Ch03 and Ch06 are higher than those in the granitoids.

All the geochemical features of granitoids in the Huhetaoergai pluton are similar to those of the other three granitoids – western Huhetaoergai, Zhuxiaogubuhe and Yagan – cited from previously published data [21-22].

4.3 Sr–Nd isotopic compositions

The Rb–Sr and Sm–Nd isotopic compositions of YT-20 and YT-21 from the

Preprints (www.preprints.org) | NOT PEER-REVIEWED | Posted: 22 June 2018 doi:10.20944/preprints201806.0344.v1

granites in the Huhetaoergai pluton are listed in Table 3. The initial 87Sr/86Sr ratios, εNd(t) values, and Nd model ages are calculated with the zircon U–Pb ages obtained in this study (Table 4). The results show that the Huhetaoergai granitic pluton has high initial ($^{87}Sr/^{86}Sr$)i ratios (0.708085–0.735470), low initial (143Nd/144Nd)i ratios (0.512355–0.512666), εNd(t) values of -2.98–3.23, and old model ages (TDM2) of 732–1241 Ma.

4.4. Hf isotope compositions

A total of 39 spots from samples Ch08 and Ch22 in the Huhetaoergai pluton were selected to analyze zircon Hf isotope compositions. The results are listed in Supplementary Table 5. The ratios of $^{176}Yb/^{177}Hf$, $^{176}Lu/^{177}Hf$, and $^{176}Hf/^{177}Hf$ are 0.006393–0.025179, 0.000335–0.001233, and 0.282895–0.282951, respectively. Values of εHf(t) range from 9 to 11.05 (average 9.99). The Hf model ages (TDM2) range from 549 to 679 Ma, and (TDM) ages range from 426 to 509 Ma.

5. Discussion

5.1. Is the pluton in the northern Ya-Gan fault zone composed of S-, I-, or A-type granites?

Granitic rocks can be subdivided into I-, S-, and A-types based on their geochemical characteristics, protoliths, and tectonic settings [27-32]. The diagrams for Zr-SiO_2 and Ce-SiO_2 from the bulk rock (Fig. 7a,b) indicate that the majority of the samples in the northern Ya-Gan fault zone plot in the I-type granite area and a

Preprints (www.preprints.org) | NOT PEER-REVIEWED | Posted: 22 June 2018 doi:10.20944/preprints201806.0344.v1

small number are found in the A-type region. In addition, they have low 10000Ga/Al values (2.31–2.68; mean = 2.45), which are lower than those of typical A-type granites (Whalen 1987). In the Zr-10000Ga/Al and Y-10000Ga/Al diagrams, most of the samples plot in the field of I & S granites (Fig. 7c, d). Corundum is found in the calculation of standard minerals (Table 6), which is not consistent with S-type granite. The granitoids in the Huhetaoergai pluton have relatively low A/CNK ratios (average 0.98), and there is a negative correlation between SiO_2 and P_2O_5, which indicates that the rocks are most likely I-type granites [33-34]. Furthermore, the temperatures for these granites calculated by the model of the zircon saturation thermometer are 660°C–831°C, which are not in line with those for typical A-type granites at approximately 900°C (Fig. 8a). Consequently, these granitoids are concluded to likely be I-type granites.

5.2. Petrogenesis of the pluton in the northern Ya-Gan fault zone

5.2.1. Fractional crystallization of the pluton in the northern Ya-Gan fault zone

Within the granitoids of the pluton in the northern Ya-Gan fault zone, strong fractionation of plagioclase, biotite, and K-feldspar is indicated by negative correlations of SiO_2 with CaO, TFe_2O_3, MgO, K_2O, MnO, Na_2O, P_2O_5, and Al_2O_3 (Fig. 4). These features suggest that fractional crystallization played a major role in the magma process.

Chondrite-normalized REE plots of all samples show right-dipping oblique

Preprints (www.preprints.org) | NOT PEER-REVIEWED | Posted: 22 June 2018 doi:10.20944/preprints201806.0344.v1

trends and slightly depleted Eu, despite differences in element contents. The slope of the LREE curve is greater than that of the HREE curve, which shows that the magma has undergone differentiation and different degrees of local melting (Fig. 6a). The weak negative Eu anomalies indicate that the plagioclase in the samples has undergone dissociation and crystallization. In the partial melting process, there is residual plagioclase in the source region, or there is crystallization of plagioclase in the process of crystal differentiation (Fig. 6a).

The depletions in Ti, P, Sr, Ba, and Nb in the primitive mantle-normalized trace element patterns indicate the separation and crystallization of plagioclase, K-feldspar, apatite, ilmenite and other minerals (Fig. 6 b)

The crystallization temperatures of the granites were approximately 660–830°C (Fig. 8a); the decreasing Eu/Eu* (or negative Eu anomalies) with decreasing Sr is consistent with feldspar removal, especially plagioclase, during magma evolution [35] (Fig. 8b). There are negative correlations of Rb with Ba and Sr, suggesting the fractionation of alkali feldspar and plagioclase was extensive (Fig. 8c, d).

5.2.2. Magma source and petrogenesis of the pluton in the northern Ya-Gan fault zone

The results show that the Huhetaoergai granitic pluton has high initial ($^{87}Sr/^{86}Sr$)i ratios (0.708085–0.735470), low initial (143 Nd/144Nd)i ratios (0.512355–0.512666), εNd(t) values of -2.98–3.23, and old model ages (TDM2) of 732–1241 Ma. As shown in Fig. 9, the granitoids probably originated from juvenile crust or the mantle.

 doi:10.20944/preprints201806.0344.v1

The Mg# values for the Huhetaoergai pluton are scattered (Fig. 5d). High magnesium indicates that the mafic component is from juvenile crust or the mantle. In other words, mantle material was injected into the crust, leading the increase in Mg#. This result shows that the source of the magma in the northern Ya-Gan fault zone was mixing of crust and mantle.

Values of εHf(t) range from 9 to 11.05, which are relatively high, indicating that the magma source was juvenile crust. The variation range for εHf(t) is so narrow that there is no mixing material between the crust and added mantle. The difference in the Hf model ages (TDM2) and (TDM) and the ages of the granitoids is relatively large, which suggests that the granites experienced secondary remelting of juvenile crust but were not directly separated from the mantle. As shown in Fig. 10, the granitoids also probably originated from juvenile crust, which is discovered for the first time in this paper through the Hf isotopic compositions.

One sample with low Nd may have resulted from crustal material being mixed during the ascending process. One other sample plots in the OIB field on Fig. 10. The juvenile crust may have been evolved from OIB-type mantle magma. For the other samples, the TDM2 model ages of Hf and Nd indicate that OIB magma entered the crust and formed juvenile crust, which corresponded to a period of crustal growth.

There are diorite inclusions in hand specimens Ch03 and Ch06 that contain quartz and amphibole. Since there is no quartz in the mantle, the source area should be the crust. The minerals in inclusion and granites are the same, and the chondrite-normalized REE patterns and primitive mantle-normalized trace element

 doi:10.20944/preprints201806.0344.v1

patterns of Ch03 and Ch06 are similar to those of the granitoids, which indicates that the inclusion bodies and the granites may be considered homologous. The isotopes indicate that the granite originated from juvenile crust and that the diorites such as samples Ch03 and Ch06 were also generated from juvenile crust. In addition, the inclusion injected from the mantle contains olivine, pyroxene, amphibole or garnet and does not contain quartz, so we believe that the inclusion may be the residual material in the source area after the granite melted.

The HREEs and MREEs in Ch03 and Ch06 are high, from which we can speculate that there was much amphibole and garnet left in the source area. In addition, the mineral components of diorite are consistent with the granitoids in the pluton, indicating that the residual materials such as amphibole and garnet in the source area were captured by the magma. The presence of garnets in the source area also indicates high-grade metamorphic rocks, which are deeply buried lower crustal materials.

I-type granitoids are commonly believed to form by the partial melting of preexisting meta-igneous rocks [27] and the mixing of felsic with mafic magmas [38-42]. The Sm/Nd ratios range from 0.14~0.26, i.e., <0.3, which reflects the characteristics of the continental crust components. The loss of Sr also indicates that the rock mass may be derived from the crust. The dilution of P originated in the mantle or crust. It is generally believed that the Nb/Ta and Zr/Hf values of mantle-derived rocks are approximately 17.5 and 36, respectively, while the Nb/Ta and Zr/Hf values of continental crust-derived rocks are approximately 11 and 33, respectively [25]. The Nb/Ta and Zr/Hf of granites in the Huhetaoergai pluton are

 doi:10.20944/preprints201806.0344.v1

346 8.63~15.05 and 15.84~40.85 with averages of 11.90 and 29.11, respectively, which
347 show properties of the crust. Additionally, the loss of Nb is obvious, and we can also
348 rule out the properties of the crust.

349 The εNd values range from -5.5 to -1.1, and old model ages (TDM2) are
350 1040–1685 Ma for the three other granitoid plutons – western Huhetaoergai,
351 Zhuxiaogubuhe and Yagan – which also have high initial (87Sr/86Sr)i ratios
352 (0.707654–0.735626) and low initial (143 Nd/144Nd)i ratios (0.51136–0.512216).
353 The low εNd(t) may indicate that the source of the magma was the mantle or the
354 juvenile crust. As shown in Fig. 9a and b, the granitoids probably originated from the
355 upper continental crust or the mantle.

356 5.3. Tectonic setting of the pluton in the northern Ya-Gan
357 fault

358 In the Nb vs. Y and Yb vs. Ta discrimination diagrams for tectonic setting (Fig. 11a,
359 b), all of the samples fall into the VAG+syn-COLG field. In the Rb vs. Y+Nb
360 discrimination diagram for tectonic setting (Fig. 11c), all of the samples plot in the
361 VAG and post-COLG field, suggesting that they have a volcanic arc setting. Finally,
362 as illustrated by the R1 vs. R2 discrimination in Fig. 11d, an evolutionary trend from
363 pre-plate collision to syn-collision to post-orogenic and late orogenic stages is
364 observed, which is consistent with the above tectonic discrimination.

365 Thus, the magmatism evolved from arc magma to collisional magma, indicating
366 a subduction-accretion event in the northern Ya-Gan fault. However, the ocean

 doi:10.20944/preprints201806.0344.v1

represented by the Ya-Gan fault was closed before the Early Permian (283.2 ± 2.2 Ma) (Zheng, 2013). We speculate that the granitoids of the Huhetaoergai pluton were emplaced during an episode of intensive intraplate orogenic movement that evolved to extrusional setting after a period of extensional postcollisional intraplate evolution, and the formation mechanism of the granites was related to crustal thickening in a compressional setting.

The chondrite-normalized REE patterns and primitive mantle-normalized trace element patterns show negative anomalies for Nb, Ti and other HFSEs indicating that the granites of the pluton in the northern Ya-Gan fault zone are active continental granites with arc-related characteristics. The calcareous granodiorite magma formed by the partial melting of the overlying young crust by magma underplating.

5.4. The geodynamics of the tectono-magmatic events in the northern Ya-Gan fault zone

Recently, the formation ages of the plutons in the northern Ya-Gan fault zone have been addressed, and many stages of magma emplacement have been recorded [21] . The magmatism of the first stage produced the Neoproterozoic granites in the western Huhetaoergai pluton with an age of 889 ± 8 Ma, and these rocks are the oldest granites that crop out in this area. The second stage of magmatism involved an Early Carboniferous granodiorite with an age of 356 ± 3 Ma, which intruded into the Neoproterozoic granites. The third stage is marked by the formation of the Zhuxiaogubuhe pluton with an age of 286 ± 2 Ma, which is similar to the age of 283 ±

2 Ma in the Yagan pluton. The ages of the Huhetaoergai pluton measured in this study are 220.5 ± 1.9 Ma and 226.5 ± 2.4 Ma, which might represent the last stage of magmatism in the northern Ya-Gan fault zone (Table 4).

In the northern Ya-Gan fault belt, from west to east, the Zhuxiaogubuhe, western Huhetaoergai, Huhetaoergai and Yagan plutons are located. The long axis direction of the plutons coincides with the construction line direction, and the characteristics of the granites in each pluton are shown in Table 4.

(1) Precambrian

There are few Cambrian strata in the northern Ya-Gan tectonic zone. From the analysis of geochemistry and chronology, we can conclude the western Huhetaoergai pluton was located in a postcollision environment at 890 Ma, which resulted from the southward subduction of the Paleo-Asian Ocean and coincides with the time of the assembly of the Rodinia continent (Fig. 12a) [45-48]. As shown in Table. 3 and Table. 5, the TDM2 model age of granitoids in Huhetaoergai pluton probably range from 549-678 Ma, when a portion of basic rock is separated from the depleted mantle and remained in the lower crust with the asthenosphere intrusion mixed, during which the OIB magma entered. However, the TDM2 model age of other granitoids in western Huhetaoergai, Zhuxiaogubuhe and Yagan pluton range 1040-1685 Ma, when the asthenosphere intrusion and upper crust mixed.

(2) Carboniferous-Early Permian

The ocean represented by the Ya-Gan fault zone subducted northward and formed the Huhetaoergai volcanic arc in the Early Carboniferous when the

 doi:10.20944/preprints201806.0344.v1

410 granodiorite appeared at 356 Ma, which involved crystallization and differentiation of
411 magmas from the mixing of mantle and crust.
412 There was continuous Carboniferous deposition in the northern region, and the
413 lithology is yellow-green and fine feldspathic hard sandstones and quartz sandstones,
414 which represent the coast and shallow sea in a near-shore and oxygen-rich
415 environment. Therefore, the western Huhetaoergai pluton should have been in a
416 volcanic arc environment in the Early Carboniferous, the oceans represented by the
417 Ya-Gan fault remained open at this time, and subduction was ongoing (Fig. 12b).
418 The Zhuxiaogubuhe and Yagan plutons were generated at 286 Ma and 283 Ma,
419 respectively, in volcanic arc to postcollisional settings in the Permian; these plutons also
420 involved the crystallization and differentiation of magmas from the mixing of mantle
421 and crust (Fig. 12b).
422 (3) Late Permian-Triassic
423 Late Permian strata are widely distributed in the Huhetaoergai arc zone (HZ) and
424 the Zhusileng structural belt (ZZ) (Fig. 1) with similar lithology that represents
425 continuous coastal, shallow-sea and marine-continental environments. From the
426 perspective of regional evolution, the branch of the Paleo-Asian Ocean was closed
427 before the Early Permian (283.2 ± 2.2 Ma), which is defined by the Yagan pluton in
428 the northern part of the Alxa block [20] .
429 In this paper, two ages (220.5 Ma and 226.5 Ma) were measured in the
430 Huhetaoergai pluton, which is the latest pluton we have found. Fig. 11 shows that the
431 Huhetaoergai pluton formed in an extrusional environment, which indicates that the

 doi:10.20944/preprints201806.0344.v1

Huhetaoergai pluton represents an episode of intraplate evolution (Fig. 12c). The entire Huhetaoergai pluton underwent intensive orogenic movement in the Triassic, which led to mountain chain uplift and exhumation of subducted crust. Therefore, the Huhetaoergai pluton was in a compressional setting after a period of extensional postcollisional intraplate evolution, and the formation mechanism of the granites is related to crustal thickening in a compressional setting (Fig. 12c).

Conclusions

Based on zircon U–Pb dating, Sr–Nd–Hf isotope measurements, and major and trace element geochemistry of the Huhetaoergai granitoids in the northern Ya-Gan fault zone, together with other three studied granitoids (western Huhetaoergai, Zhuxiaogubuhe and Yagan), for which we collected previously published data, we can draw the following conclusions:

1) Zircon U–Pb dating yielded precise crystallization ages of 220.5 ± 1.9 Ma and 226.5 ± 2.4 Ma for the granitoids of the Huhetaoergai pluton in the northern Ya-Gan fault zone, which is the youngest pluton we have found in the area to date.

2) Most granitoids of the Huhetaoergai pluton are calc-alkaline to alkaline granodiorites and granites, which are similar to the rocks of the western Huhetaoergai, Zhuxiaogubuhe, and Yagan plutons.

3) The granitoids of the Huhetaoergai pluton are metaluminous to peraluminous, highly fractionated I-type granites, which are similar to the rocks of the western Huhetaoergai, Zhuxiaogubuhe, and Yagan plutons.

 doi:10.20944/preprints201806.0344.v1

453 4) High ratios (87Sr/86Sr)i, low εNd(t) values, and high εHf(t) values are
454 indicative of derivation from magma generated from juvenile crust that underwent
455 partial melting of the lower crust, and this indication is a new discovery of the source
456 for the magma in the northern Ya-Gan fault zone. However, the magmas of the
457 granitoids in the western Huhetaoergai, Zhuxiaogubuhe, and Yagan plutons are
458 products of the mixing of upper continental crust and asthenospheric materials.

459 5) The granitoids of the Huhetaoergai pluton were emplaced during an episode of
460 intense intraplate orogenic movement evolution in an extrusional setting after a period
461 of extensional postcollisional intraplate evolution, and the formation mechanism of
462 the granites is related to crustal thickening in a compressional setting.

Preprints (www.preprints.org) | NOT PEER-REVIEWED | Posted: 22 June 2018 doi:10.20944/preprints201806.0344.v1

Supplementary Materials

Figure captions

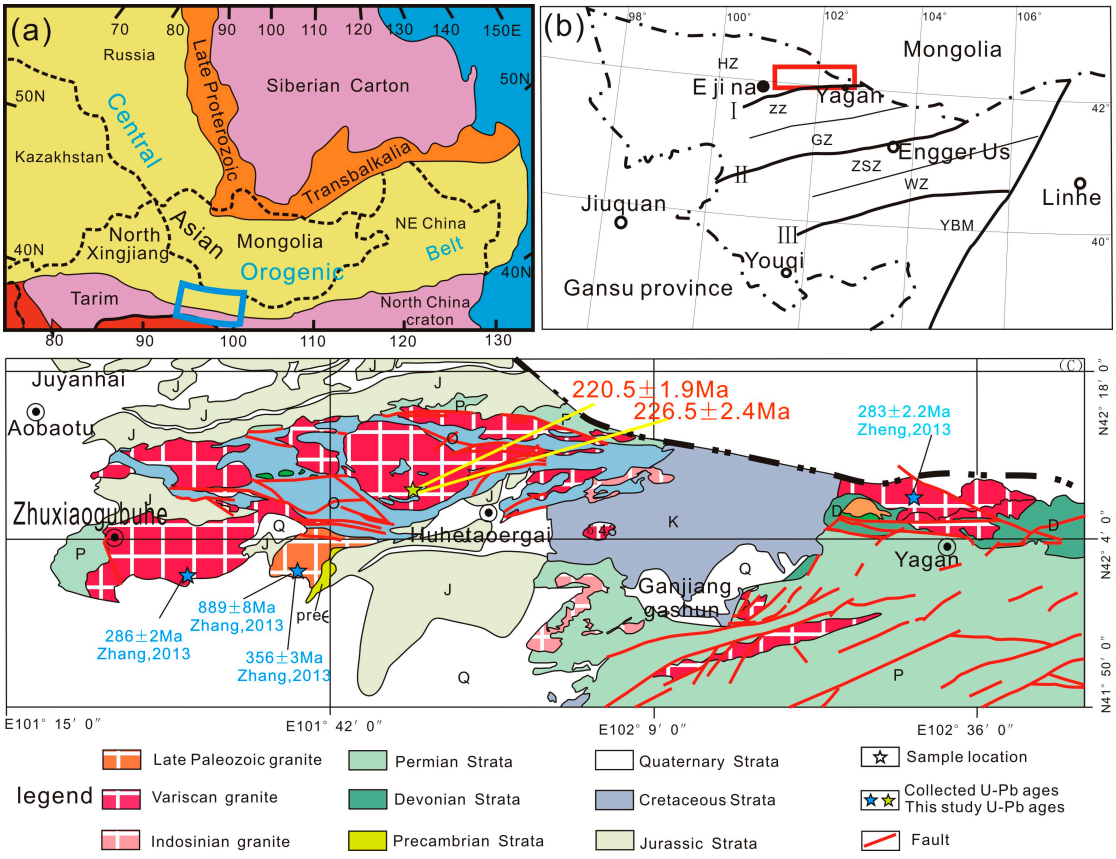

Fig. 1. (a) Tectonic location of Northern Alxa area in the Central Asian Orogenic Belt [1]. (b) Tectonic setting of the Alxa (modified after Wu and He，1993[3])(I)Yagan Fault(II)Engger Us Ophiolite Belt;(III)Qagan Qulu Ophiolite Belt.Six tectonic zones from north to south: HZ -Huhetaoergai Early Paleozoic Arc Zone, ZZ -Zhusileng EarlyPaleozoic Passive Continental Margin Zone, GZ-Guaizihu Late Paleozoic Oceanic Basin Zone, ZSZ-Zongnaishan-Shalazhashan Late Paleozoic Arc Zone, WZ-Wuliji Late Paleozoic Back-arc Basin Zone, YBM- Yabulai-Bayinnuoergong Continent Margin. (c)Simplified geological map of the Northern Alxa region [2].

Preprints (www.preprints.org) | NOT PEER-REVIEWED | Posted: 22 June 2018 doi:10.20944/preprints201806.0344.v1

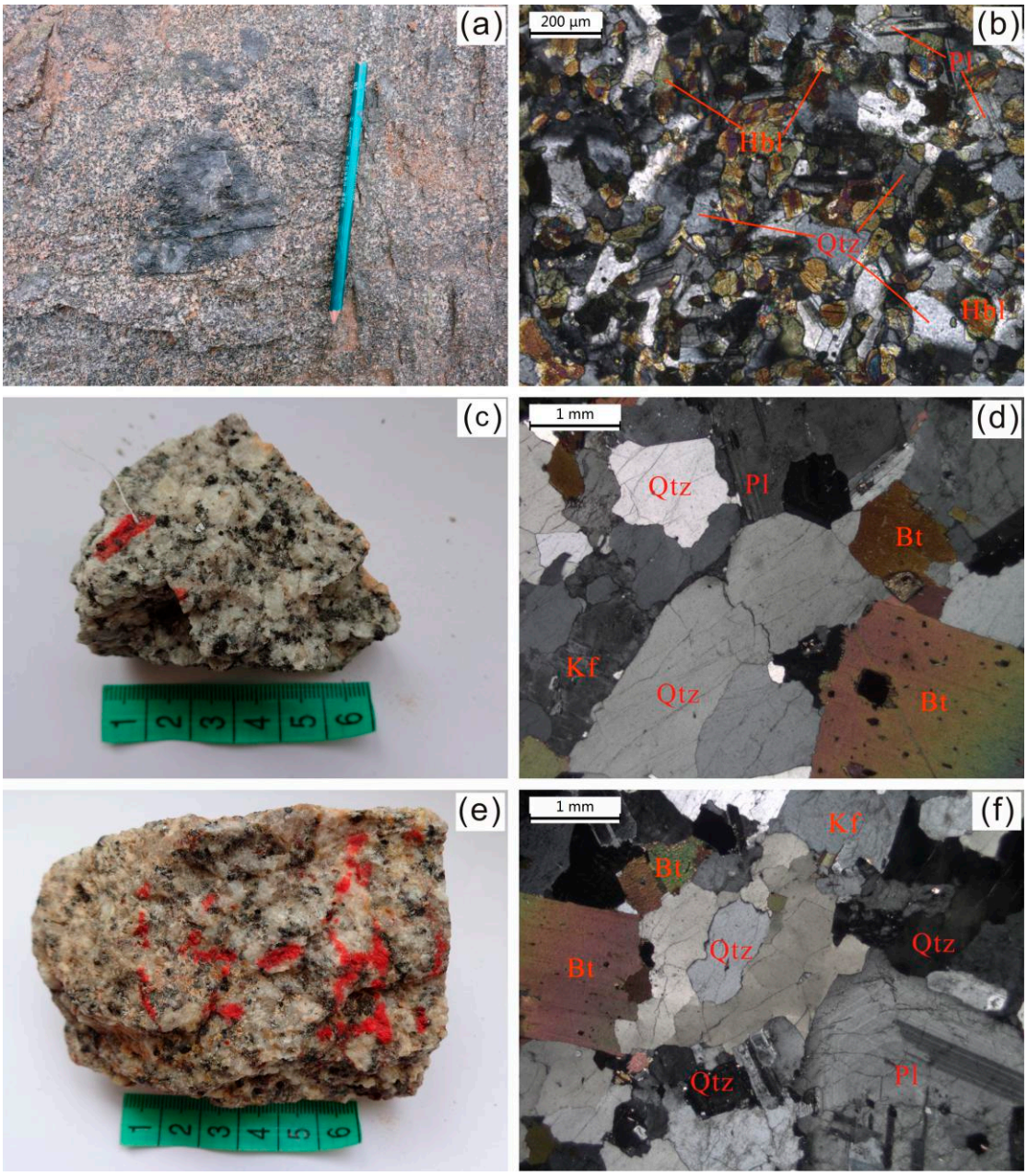

474

475 **Fig. 2** Photographs of representative rock samples and relevant photomicrographs: (a

476 and b) Hornblende diorite (xenoliths); (c and d) Medium- to coarse-grained biotite

477 adamellite; (e and f) Coarse-grained biotite adamellite with K-feldspar megacrysts.

Preprints (www.preprints.org) | NOT PEER-REVIEWED | Posted: 22 June 2018 doi:10.20944/preprints201806.0344.v1

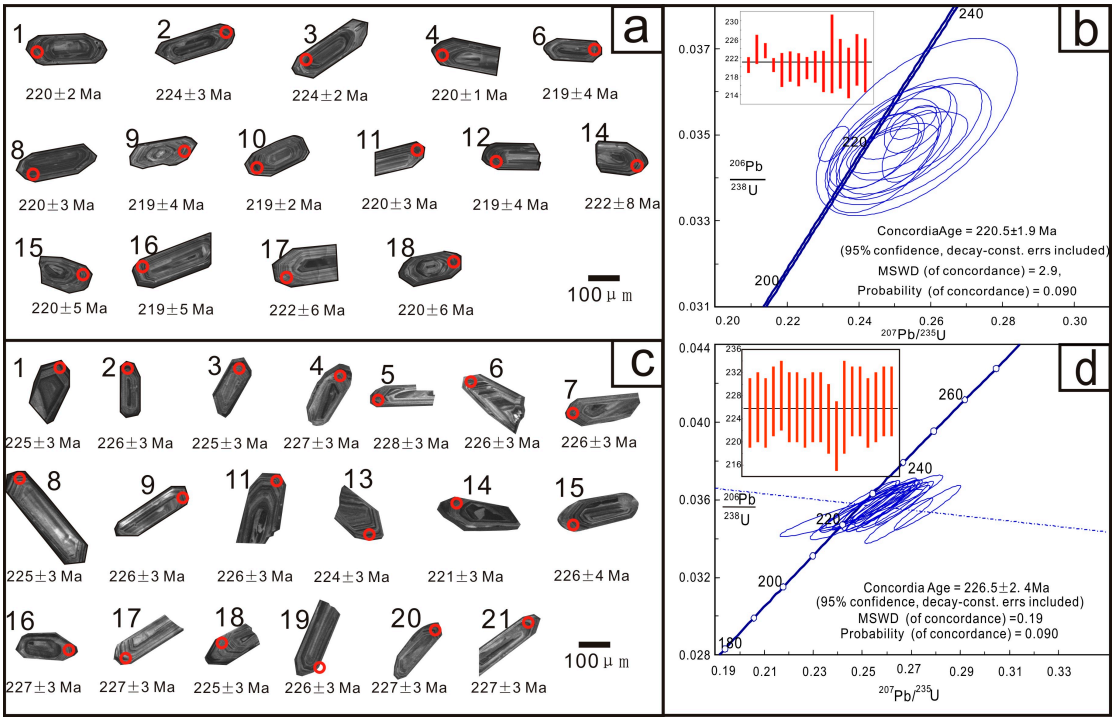

Fig. 3. Cathodoluminescence (CL) images of representative zircon grains and concordia diagrams of zircon U–Pb geochronological data for the samples Ch08 and Yh22 from the Huhetaoergai pluton.

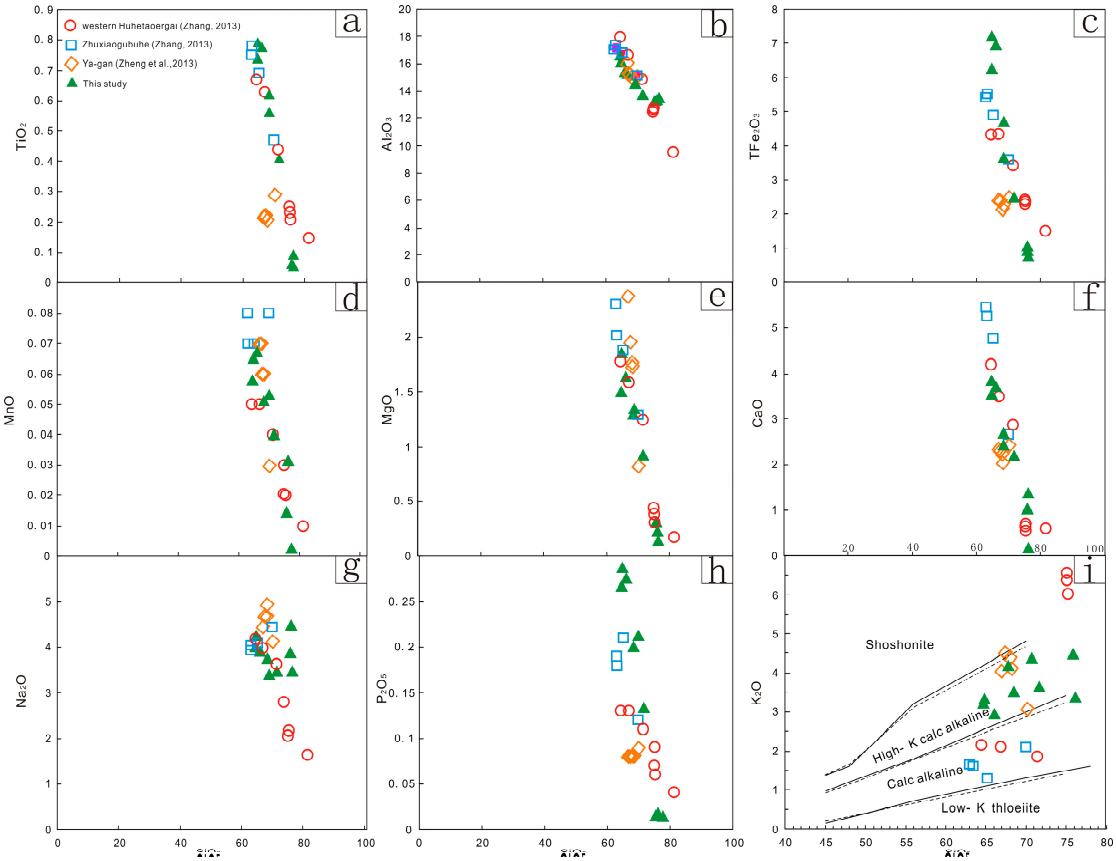

Preprints (www.preprints.org) | NOT PEER-REVIEWED | Posted: 22 June 2018 doi:10.20944/preprints201806.0344.v1

Fig. 4. Geochemical plots of the granitic rocks from the Huhetaoergai granitic pluton in the northern Ya-Gan fault zone. Fig. 4i is modified from [22].

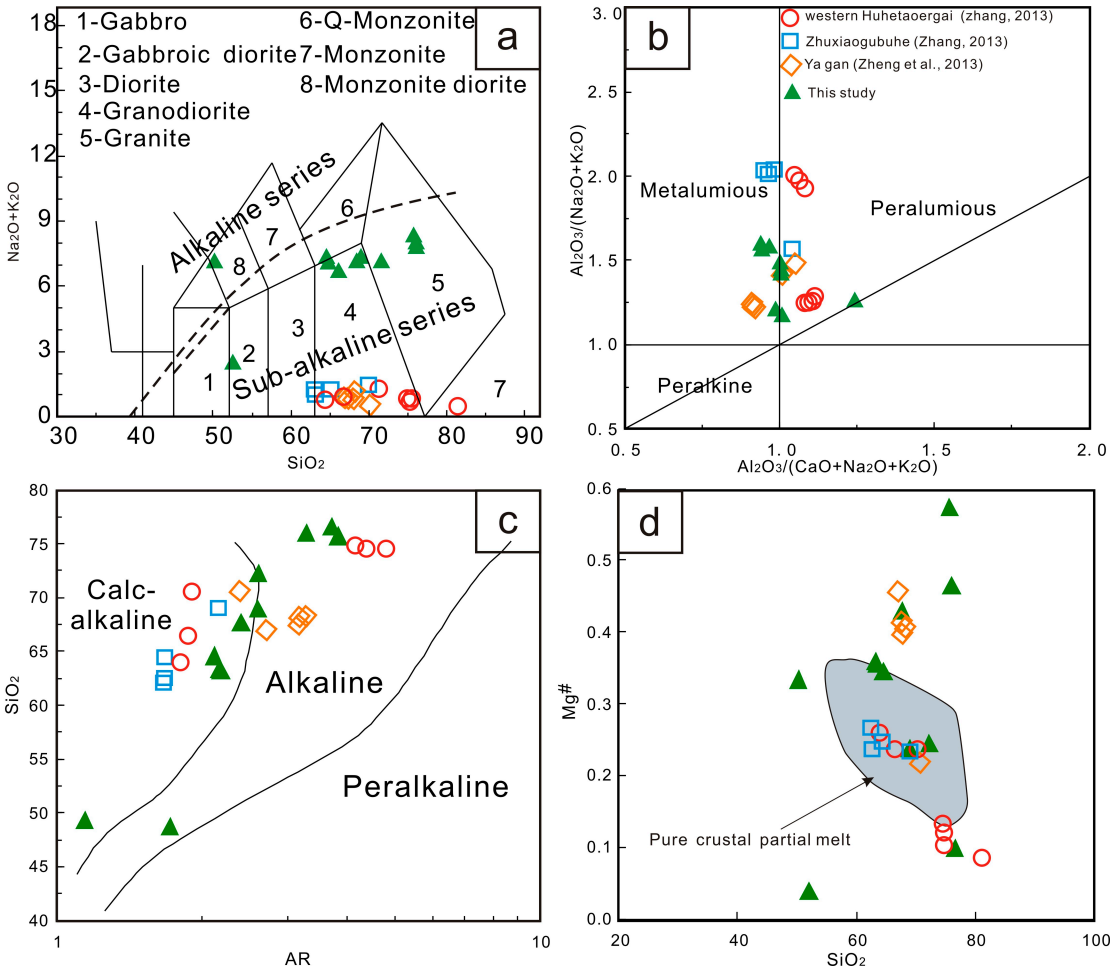

Fig. 5. a. Major and trace element diagrams of the granitoids: Na2O+K2O vs. SiO2 diagram [23] **b**. Al_2O_3/ (Na_2O+K_2O) vs. Al_2O_3/ ($CaO+Na_2O+K_2O$). (the discrimination diagram is after Maniar and Piccoli, 1989[24])

c. AR vs.SiO2 ,where AR (Alkalinity Ratio)=[Al2O3+CaO+(Na2O+K2O)]/[Al2O3+CaO−(Na2O+K2O)] (wt.%).

d. Mg# [=Mg/(Mg+FeT)] vs. SiO2 diagram.

Preprints (www.preprints.org) | NOT PEER-REVIEWED | Posted: 22 June 2018 doi:10.20944/preprints201806.0344.v1

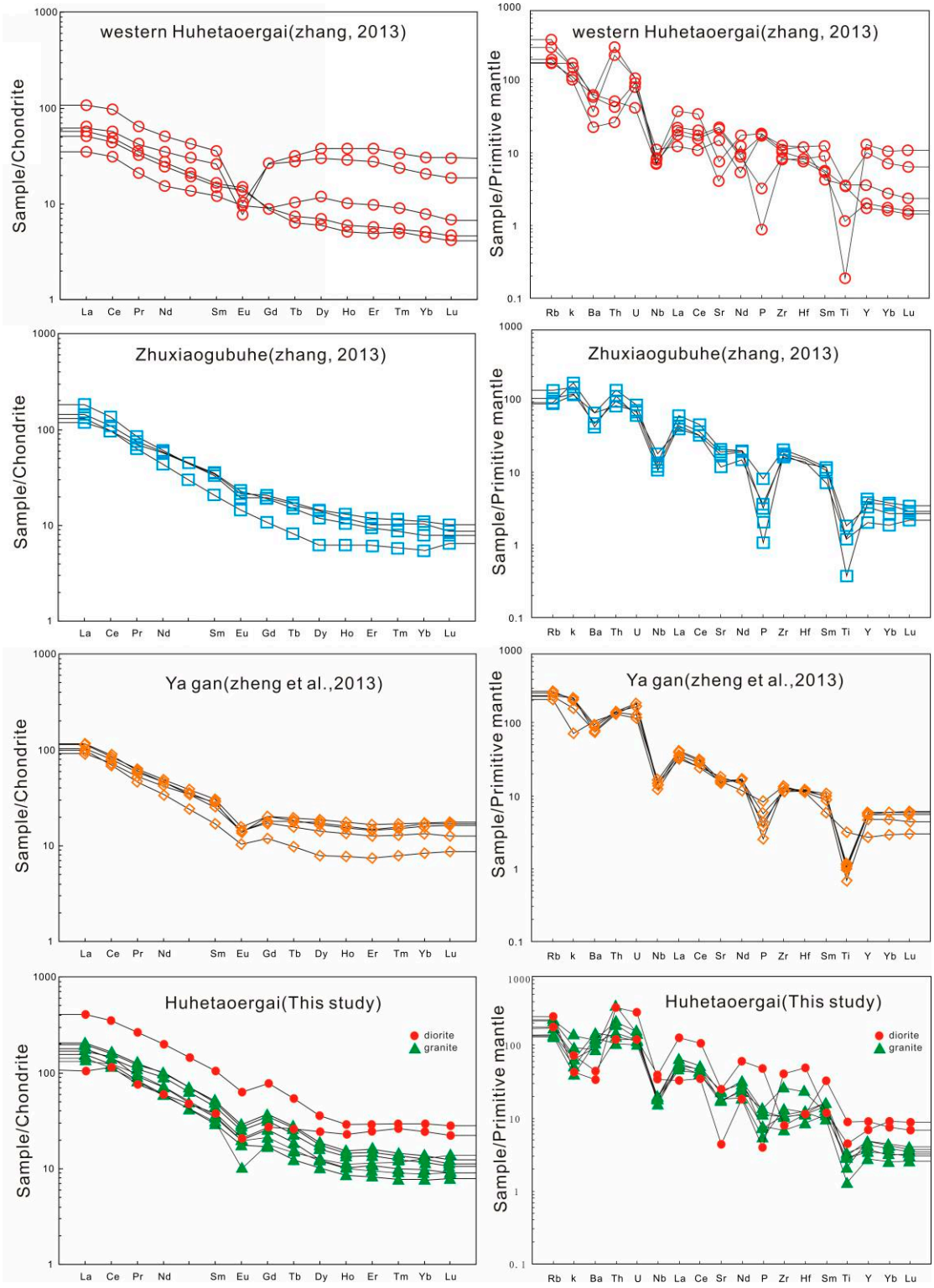

493

494 **Fig. 6.** (a) Chondrite-normalized REE chemistry and (b) primitive-mantle-normalized

495 incompatible trace element variation diagram for the samples taken from the pluton in

496 the northern Ya-Gan fault zone. Normalizing factors are from Taylor and McLennan

497 (1985) [25] and Sun and McDonough (1989) [26], respectively.

Preprints (www.preprints.org) | NOT PEER-REVIEWED | Posted: 22 June 2018 doi:10.20944/preprints201806.0344.v1

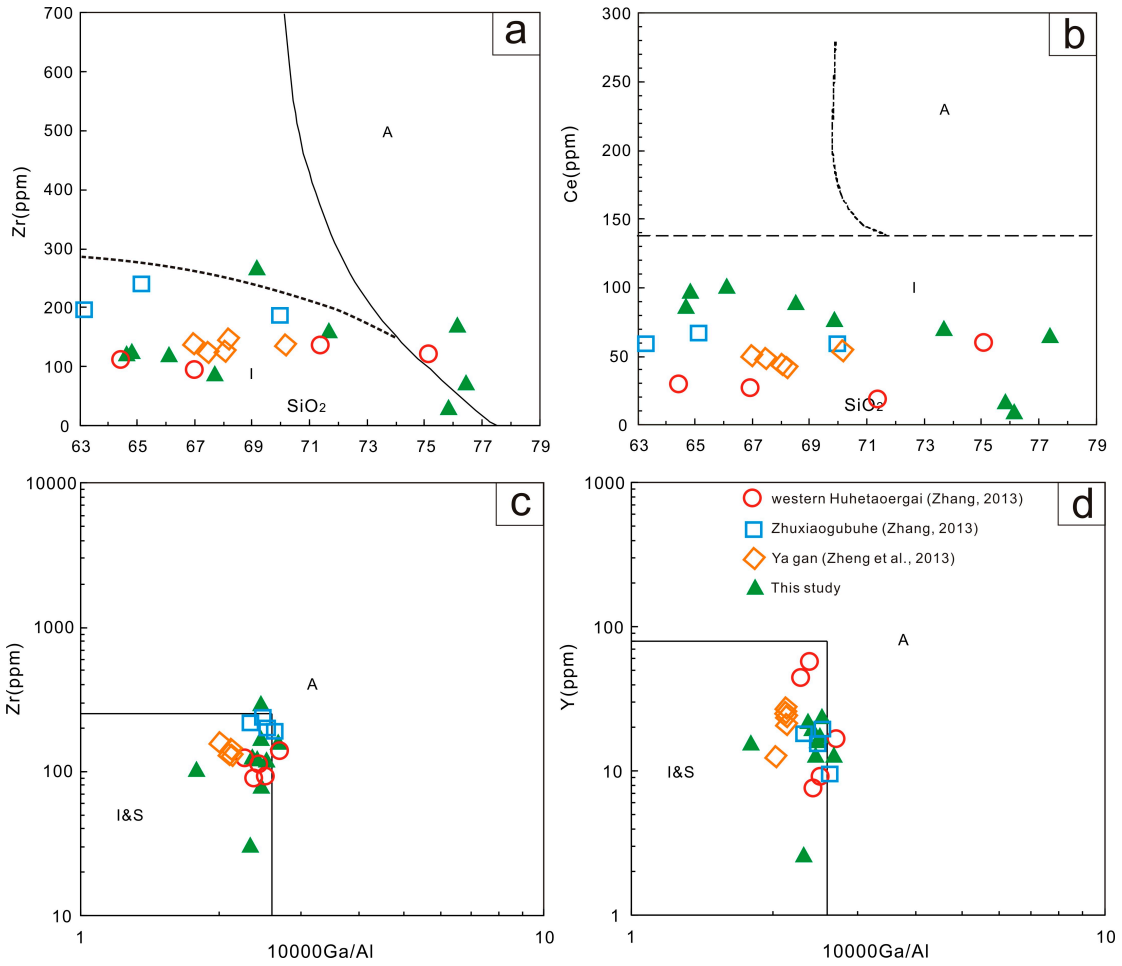

498

499 **Fig. 7.** (a) Zr vs. SiO2 diagram; (b) Ce vs. SiO2 diagram ; (c) Y versus 10,000 Ga/Al

500 diagram and (d) Zr versus 10,000 Ga/Al diagram for the samples taken from the

501 pluton in the northern Ya-Gan fault zone. The discrimination diagrams are after

502 Whalen et al. (1987) [31].

Preprints (www.preprints.org) | NOT PEER-REVIEWED | Posted: 22 June 2018 doi:10.20944/preprints201806.0344.v1

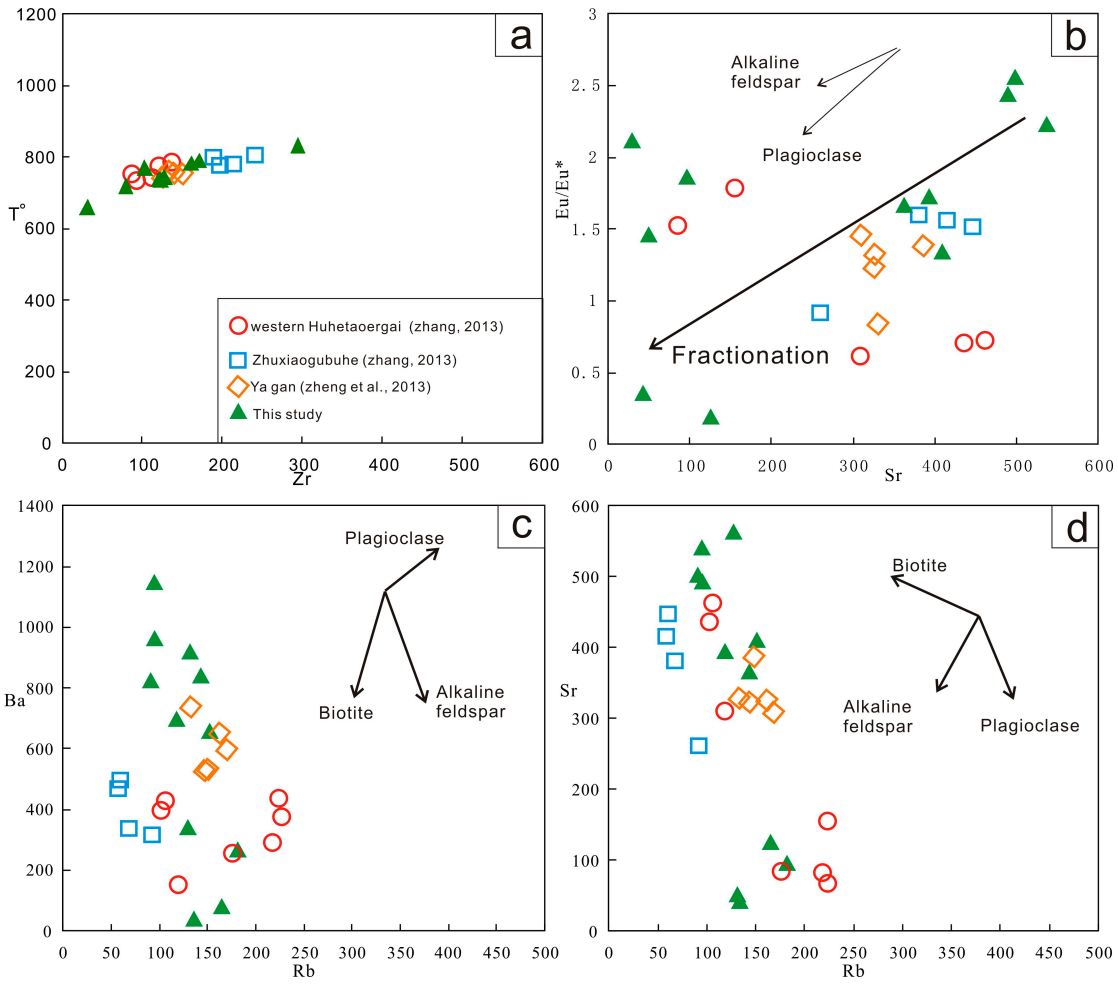

503

504 **Fig. 8.** Fractional crystallization vector diagrams for the samples taken fro the pluton

505 in the northern Ya-Gan fault zone:(a) diagram for variations of saturation temperatures

506 in bulk-rock;(b) Eu/Eu*versus Sr diagram (c) Ba versus Rb diagram (d) Sr versus Rb

507 diagram.

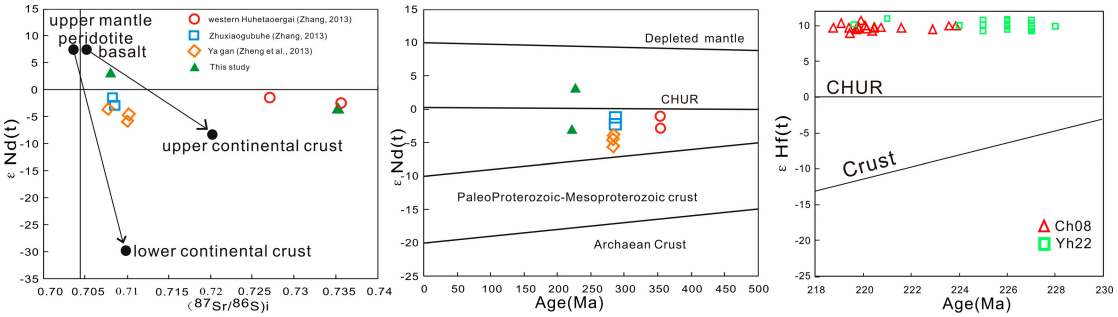

508

509 **Fig. 9.** (a) εNdt vs. (87Sr/86Sr)i ratios. Two end-members: depleted mantle or

510 juvenile components [36]. (b) eNdt vs. intrusive age of the pluton in the northern

Preprints (www.preprints.org) | NOT PEER-REVIEWED | Posted: 22 June 2018 doi:10.20944/preprints201806.0344.v1

511 Ya-Gan fault zone. (c) εHf(t) vs. Age figure.

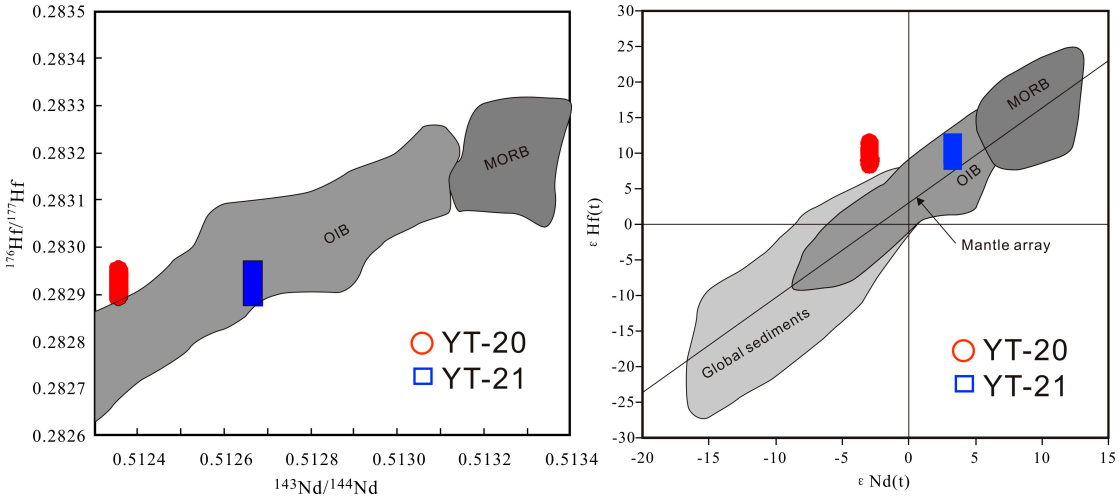

512

513 **Fig. 10a**.The diagram of$^{143}Nd/^{144}Nd$ vs.$^{176}Hf/^{177}Hf$; b. The diagram of initial εNd(t)

514 vs. Initial εHf(t) showing Nd–Hf decoupling of studied samples Data source: MORB,

515 OIB, and global sediments [37]

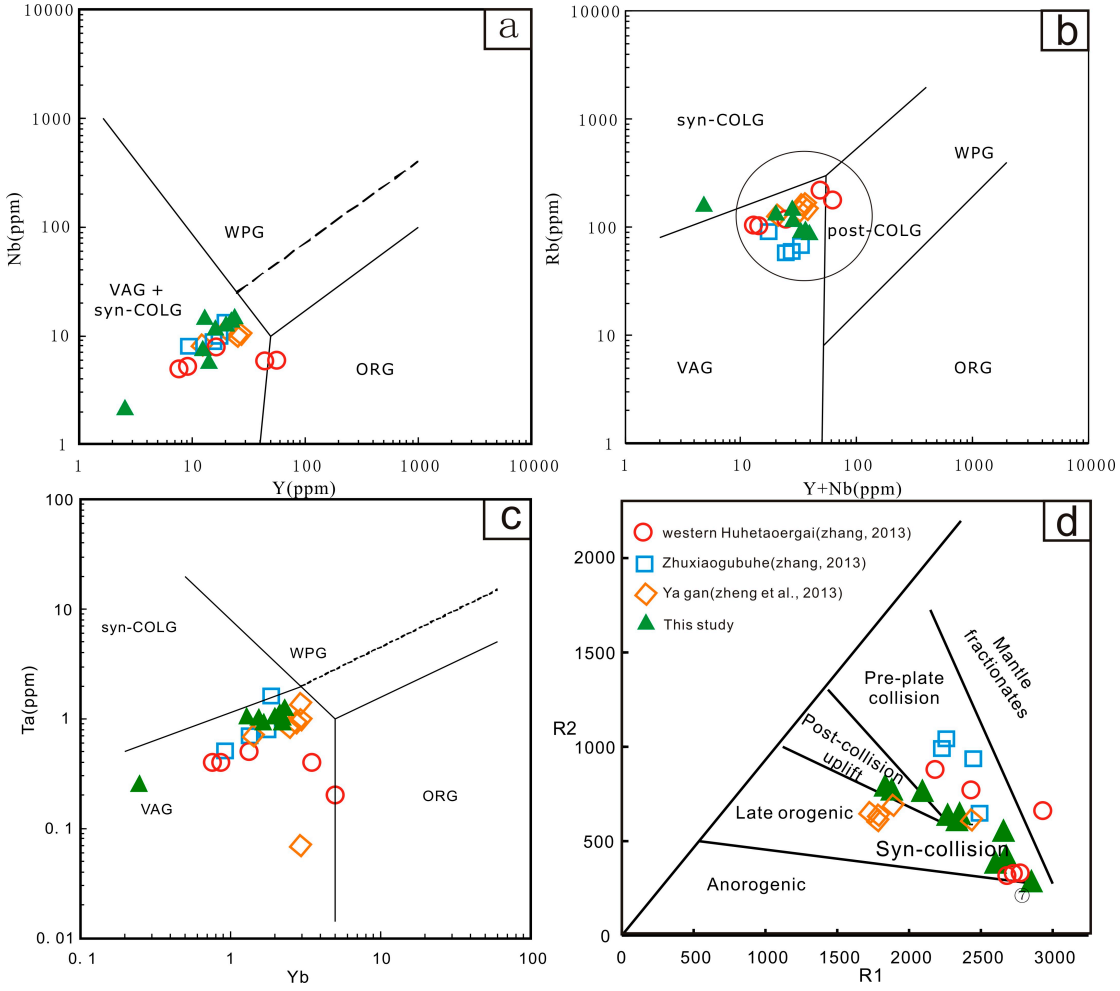

516

 doi:10.20944/preprints201806.0344.v1

517 **Fig. 11.** Discrimination diagrams for tectonic setting of (a) Nb vs. Y [43]; (b) Rb vs.
518 Y+Nb[44]; (b) Yb vs. Ta [43]; (d) R1 vs. R2 (R1=4Si−11 (Na + K)−2 (Fe+Ti),
519 R2=6Ca+2Mg+Al; [44]). Abbreviations: VAG, volcanic-arc granitoids; Syn-COLG,
520 syn-collisional granitoids;WPG, within-plate granitoids; ORG, ocean-ridge granitoids;
521 OIB, ocean island basalt; and MORB, mid-ocean ridge basalt. POG-post-collision
522 granites

Preprints (www.preprints.org) | NOT PEER-REVIEWED | Posted: 22 June 2018 doi:10.20944/preprints201806.0344.v1

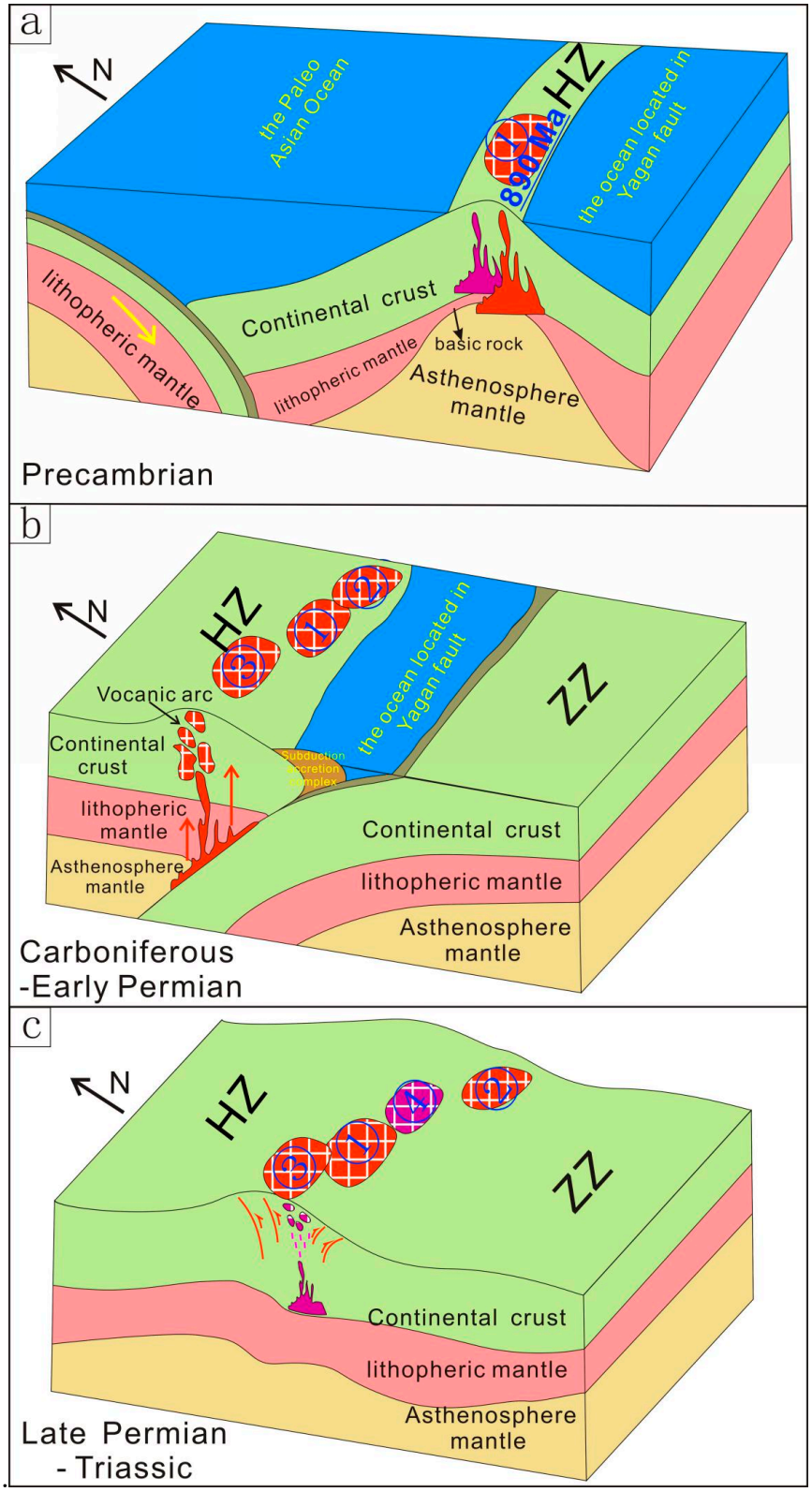

523

524 **Fig. 12.** Schematic model for the tectonic evolution of granitic pluton in the northern

525 Ya-Gan fault zone during Precambrian–Triassic.（HZ -Huhetaoergai Early Paleozoic

 doi:10.20944/preprints201806.0344.v1

Arc Zone, ZZ -Zhusileng EarlyPaleozoic Passive Continental Margin Zone ①western Huhetaoergai granodiorite pluton② Yagan grained biotite adamellite pluton ③Zhuxiaogubuhe granite pluton④Huhetaoergai pluton）

Table captions

Table 1 LA-ICP-MS zircon U–Pb data of the granites in Huhetaoergai pluton

Table 2 Whole rock chemical compositions of the granite in Huhetaoergai pluton

Table 3 Whole rock Sr–Nd isotopic compositions

Table 4 The characteristic of different granitic plutons in the northern Ya-Gan fault zone

Table 5 Zircon Hf isotopic compositions of Ch08 and Yh22 from granites in Huhetaoergai pluton .

Table 6 CIPW standard mineral and petrochemical parameters calculation in the granites of Huhetaoergai pluton

Table 1 LA-ICP-MS zircon U–Pb data for the granites in the Huhetaoergai pluton

spot	^{232}Th (ppm)	^{238}U (ppm)	^{232}Th/^{238}U	^{207}Pb/^{206}Pb		^{207}Pb/^{235}U		^{206}Pb/^{238}U		^{208}Pb/^{232}Th		^{207}Pb/^{206}Pb		^{207}Pb/^{235}U		^{206}Pb/^{238}U	
				Ratio	1sigma	Ratio	1sigma	Ratio	1sigma	Ratio	1sigma	Age (Ma)	1sigma	Age (Ma)	1sigma	Age (Ma)	1sigma
Ch08-1	902.02	1227.44	0.73	0.0486	0.0005	0.2331	0.0028	0.0348	0.0003	0.0005	0.0001	127.9	24	212.7	2	220.5	2
Ch08-2	366.09	368.14	0.99	0.0527	0.0012	0.2563	0.0061	0.0353	0.0005	0.0007	0.0002	316.7	54	231.7	5	223.9	3
Ch08-3	197.65	249.55	0.79	0.0524	0.0008	0.2552	0.0043	0.0353	0.0003	0.0010	0.0002	301.9	6	230.8	3	223.6	2
Ch08-4	281.23	343.10	0.82	0.0518	0.0011	0.2490	0.0056	0.0348	0.0002	0.0008	0.0002	279.7	46	225.8	5	220.5	1
Ch08-6	390.57	586.59	0.67	0.0513	0.0017	0.2451	0.0087	0.0346	0.0006	0.0008	0.0003	253.8	69	222.6	7	219.4	4
Ch08-8	138.27	224.52	0.62	0.0528	0.0017	0.2540	0.0108	0.0347	0.0005	0.0018	0.0005	320.4	69	229.8	9	220.1	3
Ch08-9	142.25	190.86	0.75	0.0515	0.0013	0.2456	0.0073	0.0346	0.0006	0.0010	0.0003	264.9	55	223.0	6	219.4	4
Ch08-10	116.65	141.37	0.83	0.0521	0.0016	0.2494	0.0084	0.0347	0.0004	0.0012	0.0004	300.1	72	226.1	7	219.8	2
Ch08-11	572.95	618.47	0.93	0.0532	0.0007	0.2545	0.0052	0.0347	0.0006	0.0005	0.0001	338.9	30	230.2	4	220.1	3
Ch08-12	228.26	250.26	0.91	0.0524	0.0018	0.2499	0.0106	0.0346	0.0007	0.0007	0.0002	301.9	78	226.5	9	219.1	4
Ch08-14	43.72	92.82	0.47	0.0521	0.0026	0.2562	0.0185	0.0352	0.0014	0.0037	0.0014	287.1	115	231.6	15	222.9	8
Ch08-15	100.49	97.36	1.03	0.0524	0.0022	0.2493	0.0119	0.0348	0.0009	0.0010	0.0003	301.9	92	226.0	10	220.7	5
Ch08-16	443.61	337.40	1.31	0.0522	0.0014	0.2472	0.0104	0.0345	0.0009	0.0004	0.0001	294.5	68	224.3	8	218.7	5
Ch08-17	249.01	211.17	1.18	0.0526	0.0018	0.2540	0.0134	0.0350	0.0009	0.0003	0.0001	322.3	78	229.8	11	221.6	6
Ch08-18	94.93	153.93	0.62	0.0532	0.0025	0.2538	0.0153	0.0348	0.0009	0.0008	0.0003	338.9	107	229.7	12	220.4	6
Yh22-01	277.43	415.72	0.67	0.0536	0.0013	0.2625	0.0062	0.0356	0.0005	0.0120	0.0003	352.0	29	237.0	5	225.0	3
Yh22-02	106.20	209.20	0.51	0.0512	0.0017	0.2520	0.0080	0.0357	0.0005	0.0121	0.0004	251.0	47	228.0	7	226.0	3
Yh22-03	214.55	295.62	0.73	0.0511	0.0015	0.2507	0.0073	0.0356	0.0005	0.0111	0.0003	245.0	41	227.0	6	225.0	3
Yh22-04	194.57	314.18	0.62	0.0506	0.0012	0.2496	0.0059	0.0358	0.0005	0.0114	0.0003	222.0	30	226.0	5	227.0	3

doi:10.20944/preprints201806.0344.v1

Yh22-05	318.74	434.81	0.73	0.0522	0.0011	0.2586	0.0055	0.0359	0.0005	0.0119	0.0002	293.0	25	234.0	4	228.0	3
Yh22-06	296.52	439.86	0.67	0.0514	0.0012	0.2523	0.0059	0.0356	0.0005	0.0116	0.0003	258.0	30	228.0	5	226.0	3
Yh22-07	382.53	674.34	0.57	0.0512	0.0011	0.2515	0.0054	0.0356	0.0005	0.0110	0.0002	250.0	26	228.0	4	226.0	3
Yh22-08	244.26	349.02	0.70	0.0526	0.0012	0.2578	0.0060	0.0356	0.0005	0.0120	0.0003	310.0	29	233.0	5	225.0	3
Yh22-09	428.43	447.89	0.96	0.0563	0.0011	0.2766	0.0056	0.0356	0.0005	0.0115	0.0002	465.0	23	248.0	4	226.0	3
Yh22-11	130.54	234.14	0.56	0.0524	0.0014	0.2581	0.0067	0.0357	0.0005	0.0119	0.0003	303.0	33	233.0	5	226.0	3
Yh22-13	409.03	567.23	0.72	0.0504	0.0026	0.2456	0.0119	0.0353	0.0005	0.0111	0.0001	215.0	118	223.0	10	224.0	3
Yh22-14	675.11	729.22	0.93	0.0550	0.0012	0.2650	0.0057	0.0349	0.0005	0.0123	0.0002	413.0	25	239.0	5	221.0	3
Yh22-15	188.34	293.65	0.64	0.0521	0.0024	0.2558	0.0111	0.0356	0.0007	0.0121	0.0004	289.0	64	231.0	9	226.0	4
Yh22-16	141.73	259.89	0.55	0.0519	0.0015	0.2560	0.0072	0.0358	0.0005	0.0116	0.0003	280.0	39	231.0	6	227.0	3
Yh22-17	303.78	389.22	0.78	0.0526	0.0011	0.2599	0.0053	0.0358	0.0005	0.0119	0.0002	312.0	24	235.0	4	227.0	3
Yh22-18	275.21	379.95	0.72	0.0524	0.0011	0.2567	0.0054	0.0355	0.0005	0.0119	0.0003	302.0	25	232.0	4	225.0	3
Yh22-19	341.61	466.85	0.73	0.0534	0.0011	0.2633	0.0056	0.0358	0.0005	0.0116	0.0002	346.0	25	237.0	4	226.0	3
Yh22-20	399.94	553.37	0.72	0.0512	0.0010	0.2535	0.0048	0.0359	0.0005	0.0114	0.0002	252.0	22	229.0	4	227.0	3
Yh22-21	480.17	647.16	0.74	0.0541	0.0010	0.2672	0.0048	0.0358	0.0005	0.0117	0.0002	374.0	20	240.0	4	227.0	3

doi:10.20944/preprints201806.0344.v1

Preprints (www.preprints.org) | NOT PEER-REVIEWED | Posted: 22 June 2018 doi:10.20944/preprints201806.0344.v1

Table 2. Whole rock chemical compositions of the granite in Huhetaoergai pluton

Sample no.	Ch-01	Ch-02	Ch-03	Ch-04	Ch-05	Ch-06	Ch-07	Ch-08	Yh22	YT-20	YT-21
SiO2	75.84	68.51	52.00	64.84	76.15	50.23	64.68	66.10	71.68	76.61	68.98
Al_2O_3	13.23	14.92	31.65	16.11	13.36	18.95	16.51	15.41	13.74	13.41	14.50
Fe_2O_3	0.76	3.31	8.98	4.63	0.56	9.99	4.17	4.50	2.44	1.02	3.66
MgO	0.31	1.29	0.36	1.85	0.23	3.26	1.50	1.63	0.93	0.13	1.33
CaO	1.03	2.68	0.25	3.55	1.37	6.37	3.82	3.72	2.19	0.16	2.43
Na_2O	3.88	3.75	0.75	3.98	4.47	4.95	4.25	3.90	3.46	3.45	3.39
K_20	4.47	3.52	1.44	3.33	3.38	2.43	3.24	2.95	3.65	4.35	4.14
MnO	0.01	0.05	0.03	0.07	0.03	0.12	0.06	0.07	0.04	0.00	0.05
TiO_2	0.06	0.56	1.04	0.79	0.05	2.08	0.74	0.77	0.41	0.09	0.61
P_2O_5	0.01	0.20	0.07	0.29	0.02	0.84	0.27	0.28	0.13	0.01	0.21
LOI	0.38	1.15	3.30	0.56	0.36	0.71	0.71	0.64	0.52	0.75	0.72
FeO	0.18	1.32	6.75	2.55	0.20	5.02	2.10	2.39			
Total	100.16	101.26	106.62	102.54	100.17	104.96	102.04	102.36	99.19	99.96	100.03
A/NK	1.18	1.49	11.29	1.59	1.21	1.76	1.57	1.60	1.42	1.29	1.44
A/CNK	1.01	1.00	9.73	0.97	0.99	0.85	0.95	0.94	1.01	1.25	1.00
Mg#	0.57	0.43	0.04	0.36	0.46	0.33	0.36	0.34	0.24	0.10	0.24
Li	4.86	27.60	29.10	26.10	2.87	44.00	21.50	21.50	30.92		
Be	2.50	2.20	2.78	1.99	4.20	2.50	2.13	2.11			
Sc	0.98	5.97	18.70	7.88	1.84	18.80	7.76	8.86	5.17	4.86	7.49
V	9.16	69.50	157.00	87.10	3.33	221.00	80.80	88.00	49.16	3.70	65.57
Cr	0.87	14.70	123.00	11.50	0.48	6.59	11.30	12.30	17.13	2.46	36.93
Co	1.10	7.57	13.70	9.42	0.22	21.10	9.18	9.96	5.93	0.35	7.66
Ni	0.42	5.92	56.40	4.90	0.14	3.93	4.93	5.40	8.93	1.10	7.06
Cu	5.23	14.10	0.80	16.90	2.10	39.20	17.80	18.20	13.10	1.59	16.69
Zn	13.90	66.30	51.80	75.80	15.00	153.00	69.60	78.40	50.90	43.18	62.94
Ga	16.20	19.30	39.80	20.10	17.30	31.10	20.90	20.50	19.73	12.64	18.95
Rb	165.00	119.00	182.00	95.10	135.00	128.00	94.70	89.80	152.02	131.90	143.40
Sr	125.00	393.00	96.10	490.00	40.40	560.00	538.00	499.00	409.00	49.58	362.40
Y	2.58	16.30	34.00	22.30	12.70	43.80	20.20	23.50	13.04	15.94	17.29
Nb	2.21	11.90	28.70	14.00	7.51	31.00	12.90	15.40	14.74	10.98	12.76
Mo	0.36	0.54	2.08	0.71	0.46	2.58	1.36	1.96			
Cd	0.01	0.04	0.04	0.05	0.05	0.07	0.04	0.07			
In	0.01	0.03	0.09	0.04	0.01	0.08	0.04	0.04			
Sb	0.20	0.30	0.96	0.09	0.30	0.18	0.11	0.08			
Cs	2.65	2.55	43.40	2.99	6.35	3.08	2.47	2.77	3.50	2.80	3.68
Ba	71.10	696.00	262.00	1147.00	39.30	345.00	965.00	819.00	658.00	919.70	839.60
La	15.30	39.80	24.50	47.00	4.95	96.20	42.20	48.30	37.06	33.97	32.07
Ce	16.90	89.10	70.10	97.40	9.95	211.00	86.70	101.00	75.94	71.84	76.34
Pr	1.21	8.71	7.20	11.40	1.08	24.70	10.40	11.90	7.90	7.90	9.26

Preprints (www.preprints.org) | NOT PEER-REVIEWED | Posted: 22 June 2018 doi:10.20944/preprints201806.0344.v1

Nd	3.53	33.10	27.40	47.00	4.07	91.70	42.30	46.70	27.60	27.61	33.65
Sm	0.50	5.24	5.73	7.54	1.06	16.00	6.85	7.78	4.49	4.84	5.54
Eu	0.16	1.16	1.20	1.58	0.25	3.63	1.46	1.66	1.02	0.60	1.15
Gd	0.66	5.22	5.52	7.20	1.02	15.90	6.51	7.70	3.47	3.86	4.38
Tb	0.07	0.70	0.97	1.00	0.21	2.02	0.86	1.03	0.46	0.57	0.58
Dy	0.35	3.14	6.16	4.49	1.62	8.96	4.03	4.76	2.57	3.25	3.11
Ho	0.07	0.58	1.30	0.82	0.39	1.62	0.75	0.87	0.49	0.65	0.60
Er	0.23	1.78	4.05	2.46	1.33	4.88	2.26	2.65	1.37	1.92	1.59
Tm	0.04	0.26	0.73	0.35	0.30	0.67	0.32	0.37	0.20	0.31	0.24
Yb	0.25	1.67	4.83	2.15	2.24	4.15	1.99	2.31	1.30	2.23	1.55
Lu	0.05	0.23	0.71	0.29	0.39	0.56	0.27	0.31	0.20	0.36	0.24
Ta	0.26	0.93	2.22	1.15	1.03	2.06	1.07	1.26	1.05	0.93	1.04
W	0.75	0.68	1.73	0.35	0.63	1.03	0.28	0.31			
Re	<0.002	0.00	0.01	0.00	0.00	0.01	0.00	0.00			
Tl	0.76	0.58	4.05	0.48	0.61	0.67	0.46	0.45		472.20	3682.40
Pb	28.00	19.60	13.90	14.70	48.40	14.50	18.40	15.10	20.46	19.09	19.91
Bi	0.19	0.43	0.43	0.17	0.43	0.27	0.20	0.32			
Th	20.60	33.10	32.60	12.30	16.80	11.60	9.83	13.90	18.08	12.70	17.90
U	1.04	3.27	6.74	2.59	6.59	2.82	2.33	2.69	2.81	2.37	3.27
Zr	31.20	79.50	505.00	128.00	171.00	97.70	123.00	121.00	161.03	103.40	294.70
Hf	1.97	2.82	16.90	4.08	7.07	3.80	3.66	3.74	3.94	3.91	7.33
ΣREE	39.30	190.68	160.40	230.67	28.86	481.99	206.90	237.34	164.08	159.91	170.29
LREE	37.60	177.11	136.13	211.92	21.36	443.23	189.91	217.34	154.02	146.76	158.02
HREE	1.71	13.57	24.27	18.75	7.50	38.76	16.99	20.00	10.06	13.16	12.28
LREE/HREE	22.03	13.05	5.61	11.30	2.85	11.44	11.18	10.87	15.31	11.15	12.87
δEu	0.85	0.67	0.64	0.65	0.71	0.69	0.66	0.65	0.76	0.41	0.69
δCe	8.20	4.69	3.42	3.62	2.62	3.46	3.56	3.59	5.15	4.47	4.17
(La/Yb)N	41.69	16.10	3.43	14.77	1.49	15.66	14.33	14.13	19.29	10.29	14.02
(La/Sm)N	19.38	4.78	2.69	3.92	2.94	3.78	3.88	3.91	5.19	4.41	3.64
(Gd/Yb)N	2.15	2.53	0.39	2.71	0.37	3.11	2.65	2.70	2.17	1.40	2.30
YbN	1.00	6.73	19.48	8.67	9.03	16.73	8.02	9.31	5.23	9.00	6.23
10000Ga/Al	2.31	2.44	2.38	2.36	2.45	3.1	2.39	2.51	2.68	1.78	2.47

Notes:Major compositions in wt.% and trace elements in ppm. LOI = lost on ignition. A/NK = molar ratios $Al_2O_3/(Na_2O+K_2O)$; A/CNK = molar ratios $Al_2O_3/(Na_2O+K_2O+CaO)$.

Table 3.Whole-rock Sr–Nd isotope compositions

pluton	Sample no.	Rb	Sr	Sm	Nd	87Rb/86Sr	87Rb/86Sr（±2σ）	（87Sr/86Sr）t	147Sm/144Nd	143Nd/144Nd（±2σ）	(143Nd/144Nd)t	εNd(0)	εNd(t)	fSm/Nd	TDM1 (Ma)	TDM2 (Ma)	Reference
Huhetaoergai	YT-20	131.9	49.58	4.844	27.61	7.72	0.711370	0.73547	0.1061	0.512202	0.512355	-5.52	-2.98	-0.46	1128	1241	This study
	YT-21	143.4	362.4	5.543	33.65	1.14	0.704500	0.708085	0.0996	0.512523	0.512666	0.55	3.28	-0.49	649	732	
western Huhetaoergai	AB10-41	170.6	87.6	4.79	17.5	5.69	0.807850	0.735626	0.1649	0.512321	0.51136	-6.19	-2.6	-0.16	2452	1685	
	AB10-49	222.3	161.4	6.42	28.3	4.01	0.778228	0.727305	0.1368	0.512236	0.511439	-7.85	-1.1	-0.3	1707	1546	
Zhuxiaogubuhe	W08-168	57.2	452.6	6.12	35.5	0.37	0.709946	0.708462	0.1041	0.51236	0.512166	-5.42	-2	-0.47	1013	1119	Zhang et al., 201
	W08-170	52.8	414.1	5.75	30.8	0.37	0.709866	0.70837	0.1127	0.512426	0.512216	-4.14	-1.1	-0.43	1000	1040	
Yagan	W08-274	150.8	298.4	3.84	16.8	1.46	0.716136	0.710237	0.1385	0.512249	0.511992	-7.6	-5.5	-0.3	1821	1492	
	W08-276	139	306.4	3.64	24.5	1.31	0.715411	0.710116	0.09	0.512207	0.51204	-8.42	-4.6	-0.54	1162	1419	
	W08-277	125.9	302.6	2.39	13.6	1.21	0.712511	0.707654	0.1066	0.512276	0.512078	-7.06	-3.8	-0.46	1243	1357	

doi:10.20944/preprints201806.0344.v1

Table 4. The characteristic of different granitic plutons in the northern Ya-Gan fault zone

pluton	Sample no.	Lithology	Age(Ma)	Pluton occurrence	invaded formation	source region	Tectonic	References
Huhetaoergai	Ch08 Yh22	Medium- to coarse-grained biotite adamellite	220.5±1.9 226.5±2.4	>80 km^2	middle ordovician	juvenile crust	Intraplate orogenic movement in the extrusional setting after a period of extensional postcollisional	This study
western Huhetaoergai	AB10-41	Granite	889±8	80 km^2	sandstone of middle proterozoic	crust-mantle mixing	Rodinia Continental convergence	Zhang et al., 2013
	AB10-48	Granodiorite	356±3			crust-mantle mixing	Volcanic arc leding by the subduction of Yagan fault represented ocean	
Zhuxiaogubuhe	W08-170	Biotite granite	286±2	>80 km^2	middle ordovician	crust-mantle mixing	extended environment after the collision leding by the closed of Yagan fault represented ocean	Zheng et al., 2013
Yagan	W08-276	Medium grained biotite adamellite	283±2	80 km^2	upper devonian	crust-mantle mixing		

doi:10.20944/preprints201806.0344.v1

Table 5 Zircon Hf isotopic compositions for Ch08 and Yh22 from granites in the Huhetaoergai pluton .

Table.no	$\frac{^{176}Yb}{^{177}Hf}$	$\frac{^{176}Lu}{^{177}Hf}$	2σ	$\frac{^{176}Hf}{^{177}Hf}$	2σ	I_{Hf}	$\varepsilon_{Hf}(0)$	$\varepsilon_{Hf}(t)$	T_{DM}	T_{DMc}	$f_{Lu/Hf}$
Ch08-1	0.009688	0.000448	0.000020	0.282912	0.000015	0.282911	4.96	9.76	474	632	-0.99
Ch08-2	0.019752	0.000850	0.000012	0.282919	0.000015	0.282916	5.21	10.01	470	619	-0.97
Ch08-3	0.010709	0.000489	0.000016	0.282918	0.000021	0.282916	5.17	10.01	467	618	-0.99
Ch08-4	0.025031	0.001075	0.000033	0.282916	0.000026	0.282912	5.11	9.8	477	630	-0.97
Ch08-5	0.020653	0.000931	0.000075	0.282915	0.000016	0.282911	5.05	9.74	477	632	-0.97
Ch08-6	0.024035	0.001019	0.000015	0.282912	0.000014	0.282908	4.96	9.65	482	638	-0.97
Ch08-7	0.026891	0.001233	0.000028	0.282895	0.000013	0.28289	4.34	9	509	679	-0.96
Ch08-8	0.006393	0.000335	0.000003	0.282910	0.000012	0.282908	4.87	9.64	477	638	-0.99
Ch08-9	0.014673	0.000707	0.000002	0.282923	0.000014	0.28292	5.34	10.07	463	611	-0.98
Ch08-10	0.026650	0.001209	0.000027	0.282934	0.000013	0.282929	5.74	10.37	453	591	-0.96
Ch08-11	0.012055	0.000547	0.000010	0.282904	0.000013	0.282902	4.68	9.5	487	650	-0.98
Ch08-12	0.016976	0.000740	0.000010	0.282914	0.000014	0.282911	5.01	9.77	476	632	-0.98
Ch08-13	0.011790	0.000591	0.000002	0.282913	0.000015	0.282911	5	9.73	475	633	-0.98
Ch08-14	0.018739	0.000978	0.000004	0.282915	0.000015	0.28291	5.04	9.75	478	632	-0.97
Ch08-15	0.023435	0.000980	0.000074	0.282900	0.000016	0.282896	4.51	9.23	499	666	-0.97
Ch08-16	0.015934	0.000729	0.000008	0.282942	0.000017	0.282939	6.01	10.74	436	568	-0.98
Ch08-17	0.015253	0.000706	0.000004	0.282917	0.000017	0.282914	5.13	9.85	471	624	-0.98
Ch08-18	0.011859	0.000540	0.000003	0.282907	0.000013	0.282905	4.79	9.53	482	644	-0.98
Ch08-19	0.023423	0.001143	0.000026	0.282928	0.000014	0.282924	5.53	10.2	461	604	-0.97
Yh22-01	0.015319	0.000729	0.000009	0.282898	0.000013	0.282895	4.47	9.3	498	664	-0.98

doi:10.20944/preprints201806.0344.v1

Yh22-02	0.015165	0.000673	0.000002	0.282904	0.000014	0.282901	4.67	9.53	489	650	-0.98
Yh22-03	0.017291	0.000768	0.000007	0.282923	0.000012	0.28292	5.33	10.18	464	609	-0.98
Yh22-04	0.022717	0.001008	0.000014	0.282917	0.000012	0.282913	5.12	9.98	475	623	-0.97
Yh22-05	0.017199	0.000798	0.000007	0.282915	0.000011	0.282912	5.06	9.96	475	625	-0.98
Yh22-06	0.021445	0.001084	0.000017	0.282927	0.000011	0.282923	5.5	10.31	461	601	-0.97
Yh22-07	0.020458	0.000880	0.000015	0.282937	0.000014	0.282933	5.82	10.66	445	577	-0.97
Yh22-08	0.022591	0.001092	0.000021	0.282944	0.000013	0.282939	6.07	10.85	438	565	-0.97
Yh22-09	0.020010	0.000903	0.000012	0.282921	0.000013	0.282917	5.28	10.1	468	614	-0.97
Yh22-10	0.013583	0.000625	0.000016	0.282943	0.000012	0.28294	6.03	10.91	434	562	-0.98
Yh22-11	0.015482	0.000675	0.000012	0.282919	0.000012	0.282917	5.21	10.05	467	616	-0.98
Yh22-12	0.021159	0.000913	0.000012	0.282951	0.000013	0.282947	6.32	11.05	426	549	-0.97
Yh22-14	0.025179	0.001196	0.000017	0.282917	0.000016	0.282912	5.12	9.92	478	627	-0.96
Yh22-15	0.014397	0.000667	0.000005	0.282902	0.000014	0.282899	4.58	9.48	492	654	-0.98
Yh22-16	0.016373	0.000741	0.000005	0.282907	0.000012	0.282904	4.78	9.66	485	642	-0.98
Yh22-17	0.018818	0.000825	0.000014	0.282923	0.000013	0.28292	5.35	10.18	464	609	-0.98
Yh22-18	0.020239	0.000896	0.000010	0.282939	0.000012	0.282936	5.91	10.77	442	572	-0.97
Yh22-19	0.019094	0.000875	0.000007	0.282895	0.000017	0.282892	4.36	9.23	504	671	-0.97
Yh22-20	0.016607	0.000816	0.000013	0.282940	0.000014	0.282937	5.94	10.83	440	569	-0.98
Yh22-21	0.019153	0.000885	0.000018	0.282928	0.000012	0.282924	5.51	10.37	458	597	-0.97

doi:10.20944/preprints201806.0344.v1

Preprints (www.preprints.org) | NOT PEER-REVIEWED | Posted: 22 June 2018 doi:10.20944/preprints201806.0344.v1

Table 6 CIPW normative mineral and petrochemical parameter calculations for the granites of the Huhetaoergai pluton

Parameters \ Sample number	Ch-01	Ch-02	Ch-03	Ch-04	Ch-05	Ch-06	Ch-07	Ch-08	Yh22	YT-20	YT-21
Quartz(Q)	33.37	24.94	33.06	17.13	33.9		16.31	20.52	31.71	39.43	26.23
Anorthite(An)	5.08	12.25	0.84	15.85	6.42	21.47	16.2	15.58	10.42	0.92	11.05
Albite(Ab)	32.91	31.73	6.2	33.06	37.9	33.82	35.52	32.48	29.73	29.43	28.93
Orthoclase(Or)	26.48	20.8	8.28	19.32	20.02	13.82	18.91	17.16	21.89	25.91	24.7
Alkali feldspar(A)	54.09	40.77	13.91	37.48	48.72	27.06	38.04	34.18	42.03	54.33	44.69
P(Plagioclase)	10.38	24.01	1.41	30.75	15.62	42.05	32.59	31.04	20.01	1.93	19.99
Nepheline(Ne)						3.52					
Corundum(C)	0.15	0.45	27.75	0.04					0.33	2.72	0.43
Diopside(Di)					0.25	3.22	0.95	0.94			
Hypersthene(Hy)	1.25	5.54	16.09	8.29	0.88		6.37	7.31	3.36	0.79	4.79
Olives(Ol)						10.3					
Ilmenite(Il)	0.11	1.06	1.92	1.47	0.1	3.8	1.38	1.44	0.78	0.17	1.17
Magnetite(Mt)	0.61	2.77	5.64	4.2	0.48	8.14	3.73	3.94	1.44	0.63	2.18
Apatite(Ap)	0.03	0.46	0.16	0.65	0.04	1.88	0.61	0.63	0.31	0.03	0.49
Zircon(Zr)	0.01	0.02	0.1	0.03	0.03	0.02	0.02	0.02	0.03	0.02	0.06
Chromite(Cm)			0.03								0.01
Total	100	100.02	100.07	100.04	100.02	100	100	100.02	100	100.05	100.04
Differentiation index(DI)	92.76	77.47	47.54	69.51	91.82	51.16	70.74	70.16	83.33	94.77	79.86
density, g/cc	2.64	2.73	3.22	2.77	2.64	2.93	2.76	2.77	2.68	2.66	2.71
Liquid density	2.36	2.44	2.64	2.49	2.36	2.64	2.49	2.49	2.4	2.35	2.43
Dry viscosity	11.15	7.66	3.61	5.9	11.32	2.12	6.04	6.36	9.52	12.13	8.09
Wet viscosity	7.68	6.1	3.5	5.03	7.78	2.03	5.14	5.33	7.03	8.12	6.32
Liquidus temperature	737	876	1204	965	732	1244	960	939	799	716	856
H2O content	4.54	3	0.42	2.1	4.6	0.29	2.14	2.35	3.86	4.79	3.22
SI	3.28	9.88	2	11.44	2.55	12.92	9.93	10.73	8.95	1.46	10.83
AR	3.39	2.41	1.1	2.18	3.28	1.82	2.17	2.12	2.54	3.07	2.34
σ43	2.12	2.07	0.6	2.49	1.86	9.44	2.62	2.06	1.75	1.8	2.17
σ25	1.37	1.21	0.18	1.33	1.21	2.16	1.41	1.13	1.09	1.18	1.3
R1	2609	2274	2353	1885	2679	556	1837	2095	2657	2857	2335
R2	386	643	647	773	421	1169	797	769	558	289	616
F1	0.73	0.68	0.83	0.64	0.72	0.52	0.64	0.65	0.7	0.76	0.69
F2	-1.07	-1.17	-1.22	-1.21	-1.18	-1.36	-1.23	-1.24	-1.14	-1.05	-1.1
F3	-2.57	-2.52	-2.41	-2.5	-2.59	-2.46	-2.53	-2.49	-2.54	-2.55	-2.53
A/MF	6.57	1.59	1.44	1.13	8.53	0.67	1.36	1.16	2.52	8.25	1.8
C/MF	0.93	0.52	0.02	0.45	1.59	0.41	0.57	0.51	0.73	0.18	0.55

 doi:10.20944/preprints201806.0344.v1

Acknowledgments

We gratefully acknowledge American Journal Experts (AJE) for English lunguageediting. This research did not receive any specific grant from funding agencies in the public, commercial, or not-for-profit sectors.

Author Contributions

Conceptualization, Fenquan Xie , Qianhong Wu and Lidong Wang;

Methodology, Qianhong Wu and Lidong Wang;

Formal Analysis, Biao Liu and Jiangbo Jiang;

Investigation, Jiajia Song ;

Resources, Lidong Wang;

Data Curation, Fenquan Xie;

Writing–Original Draft Preparation, Fenquan Xie and Zhaoxia Shi ;

Writing–Review & Editing, Wenzhou Xiao and Jingya Cao;

Project Administration,Qianhong Wu and Lidong Wang;

Funding Acquisition, Qianhong Wu and Lidong Wang.

Conflicts of Interest:

The authors declare no conflict of interest. The founding sponsors had no role in the design of the study; in the collection, analyses, or interpretation of data; in the

writing of the manuscript, and in the decision to publish the results

References

[1] Jahn, B.M., Wu, F.Y., Chen, B. 2000a. Granitoids of the Central Asian Orogenic Belt and continental growth in the Phanerozoic. *Geological Society of America Special Papers* 350, 181 -193.

[2] Geological Survey Academy of Ningxia Hui Autonomous Region. Wuliji Regional Geological Survey Report (1:200000), 1980; Geological Survey Academy of Ningxia Hui Autonomous Region. Shalataoerhan Regional Geological Survey Report (1:200000), 1982;Geological Survey Academy of Ningxia Hui Autonomous Region. Yingen Regional Geological Survey Report (1:200000), 1980 (in Chinese).

[3] Wu, T.R., He, G.Q. 1993. Tectonic units and their fundamental characteristics on the northern margin of the Alxaa block. *Acta Geologica Sinica* 67 (2) , 98—108 (in Chinese with English abstract).

[4] Wang, T.Y., Wang, S.Z., Wang ,J.R. 1994. The Formation and Evolution of Paleozoic Continental Crust in Alxaa Region. *Lanzhou: Publishing House of Lanzhou University (in Chinese with English abstract).*

[5] Wang ,T.Y., Gao, J.P., Wang, J.R, 1998. Magmatism of collisional and post-orogenic period in Northern Alxaa Region in Inner Mongolia. *Acta Geologica Sinica* 72(2) , 126—137(in Chinese with English abstract). *Petrology* 95, 407–419.

[6] Zuo ,G.C.，Liu, Y.K. Liu, C.Y. 2003．Framework and evolution of the tectonic structure in Beishan area across Gansu Province，Xinjiang Autonomous Region and Inner Mongolia Autonomous Region． *Acta Geologica Gansu* 12(1) ,1—15 (in Chinese with English abstract).

[7] Song, J.J. 2017.Characteristics of Late Paleozoic Graniteround the Ya Gan fault zone in NorthernAlxa Block. *A Dissertation Submitted to China University of Geosciences for Master of Professional Degree* (in Chinese with English abstract).

[8] Hou, K. J., Li, Y. H., Tian, Y. Y. 2009. In situ U-Pb zircon dating using laser ablation-multi ion couting-ICP-MS. *Mineral Deposits* 28(4),481-492 (in Chinese with English abstract).

[9] Liu ,Y.S., Gao S., Hu Z.C., Gao C.G., Zong K.Q. and Wang D.B. 2010. Continental and oceanic crust recycling-induced melt-peridotite interactions in the Trans-North China Orogen: U-Pb dating, Hf isotopes and trace elements in zircons from mantle xenoliths. *Journal of Petrology* 51,537-571

[10] Nasdala L, Hofmeister W, Norberg N, Mattinson J M, Corfu F, D rr W, Kamo S L, Kennedy A K, Kronz A, Reiners P W, Frei D, Kosler J, Wan Y, G tze J, H ger T, Kr ner A & Valley J. 2008. Zircon M257 - a homogeneous natural reference material for the ion microprobe U-Pb analysis of zircon. *Geostandards and Geoanalytical Research* 32, 247-265.

[11] Sláma J, Kosler J, Condon D J, Crowley J L, Gerdes A, Hanchar J M, Horstwood M S A, Morris G A, Nasdala L, Norberg N, Schaltegger U, Schoene B, Tubrett

 doi:10.20944/preprints201806.0344.v1

M N and Whitehouse M J. 2008. Plesovice zircon — A new natural reference material for U-Pb and Hf isotopic microanalysis. *Chemical Geology* 249,1-35.

[12] Chen, F.K., Siebel, W., Satir, M., Terziog ˘lu, M., Saka, K. 2002. Geochronology of the Karadere basement (NW Turkey) and implications for the geological evolution of the Istanbul zone. *Int. J. Earth Sci* 91, 469–481.

[13] Wu, F.Y.，Yang, Y.H.，Xie, L.W. 2006a. Hf isotopic compositions of the standard zircons and baddeleyites used in U–Pb geochronology. *Chem. Geol.* 234,105~126.

[14] Hou,K.J., Li,Y.H., Zou,T.R., Qu,X.M., Shi,Y.R., Xie,G.Q. 2007. Laser ablation-MC-ICP-MS technique for Hf isotope microanalysis of zircon and its geological applications. *Acta Petrologica Sinica* 23(10), 2595-2604 (In Chinese with English abstract).

[15] Chu, N.C., Taylor, R.N., Chavagnac, V., Nesbitt, R.W., Boella, R.M., Milton, J.A., German, C.R., Bayon, G., Burton, K. 2002. Hf isotope ratio analysis using multi-collector inductively coupled plasma mass spectrometry: an evaluation of isobaric interference corrections. *J. Anal. At. Spectrom* 17, 1567–1574.

[16] Morel,M.L.A., Nebel, O., Nebel-Jacobsen, Y.J.2008. Hafnium isotope characterization of the GJ-1 zircon reference material by solution and laser-ablation MC-ICPMS. *Chemical geology* 255,231-235.

[17] Belousova, E.A., Griffin, W.L., O'Reilly, S.Y., Fisher, N.I. 2002. Igneous zircon: traceelement composition as an indicator of source rock type. *Contributions to Mineralogy and Petrology* 143, 602–622.

[18] Wu, Y.B., Zheng, Y.F., 2004. Genesis of zircon and its constraints on interpretation of U–Pb age. *Chinese Science Bulletin* 49, 1589–1604 (in Chinese with English abstract).

[19] Hoskin, P.O.W., Schaltegger, U. 2003. The composition of zircon and igneous and metamorphic petrogenesis. *Reviews in Mineralogy & Geochemistry* 53, 27–62.

[20] Zheng, R.G.，Wu ,T.R.，Zhang. W.，Feng ,J.C.，Xu, C.，Meng, Q.P. , Zhang, Z.Y. 2013. Geochronology and geochemistry of the Yagan granite in the northern margin of the Alxa block: Constraints on the tectonic evolution of the southern Altaids. *Acta Petrologica Sinica*. 29(8) ,2665－2675 1000-0569 /2013 /029(08) - 2665- 75.

[21] Zhang, W. 2013. Late paleozoic granitoids in beishan-northern alxa area (NW china) and their tectonic implications (in Chinese with English abstract).

[22] Peccerillo, A., Taylor, S. 1976. Geochemistry of Eocene calc–alkaline volcanic rocks from the Kastamonu area, northern Turkey. *Contrib. Miner. Petrol* 58, 63–81.

[23] Roger, Walter., Le, Maitre., P, Bateman., Arnošt, Dudek. 1989. A Classification of Igneous Rocks and Glossary of Terms. Blackwell, Oxford, 193.

[24] Maniar, P.D., Piccoli, P.M. 1989. Tectonic discrimination of granitoids. *Geological Society of America Bulletin* 101, 635–643.

[25] Taylor, S.R., McLennan, S.M. 1985. The Continental crust: Its composition and evolution. Boston: Blackwell Science Inc. p. 312.

[26] Sun, S.S., Mcdonough, W.F.1989. Chemical and isotopic systematics of oceanic basalts; implications for mantle composition and processes. *Geological Society London Special Publications* 42, 313–345.

[27] Chappell, B.W., White, A.J.R. 1974. Two contrasting granite types. *Pacific Geology* 8, 173–174.

[28] Chappell, B.W., White, A.J.R. 1992. I- and S-type granites in the Lachlan Fold Belt. Transactions of the Royal Society of Edinburgh. *Earth Sciences* 83, 1–26.

[29] Loiselle, M.C., Wones, D.R. 1979. Characteristics and Origin of Anorogenic Granites. Geochemical Society of America, Abstract with Programs 11, p. 468.

[30] Collins, W.J., Beams, S.D., White, A.J.R., Chappell, B.W. 1982. Nature and origin of A type granites with particular reference to southeastern Australia. *Contrib. Miner. Petrol* 80, 189–200.

[31] Whalen, J.B., Currie, K.L., Chappell, B.W. 1987. A-type granites: Geochemical characteristics discrimination and petrogenesis. *Contributions to Mineralogy and Petrology* 95, 407–419.

[32] Chappell, B.W. 1999. Aluminium saturation in I– and S–type granites and the characterization of fractionated haplogranites. *Lithos* 46, 535–551.

[33] Sylvester, P.J.1998. Post-collisional strongly peraluminous granites. *Lithos* 45, 29–44.

[34] Clemens, J.D. 2003. S-type granitic magmas-petrogenetic issues, models and evidence. *Earth-Science Reviews* 61, 1–18.

[35] Niu, Y.L., O'Hara,M.J. 2009. MORBmantle hosts themissing Eu (Sr, Nb, Ta

 doi:10.20944/preprints201806.0344.v1

and Ti) in the continental crust: new perspectives on crustal growth, crust–mantle differentiation and chemical structure of oceanic upper mantle. *Lithos* 112, 1–17.

[36] Jahn, B.M., Wu, F.Y., Hong, D.W. 2000b. Important crustal growth in thePhanerozoic: isotopic evidence of granitoids from east-central Asia. *Proceedings of the Indian Academy of Sciences (Earth and Planetary Sciences)*109, 5–20.

[37] Vervoort, J., Patchett, P.J., Blichert-Toft, J., and Albarede, F.1999.Relationships between Lu-Hf and Sm-Nd isotopic sys-tems in the global sedimentary system. *Earth and Planetary Science Letters*, v. 168, p. 79–99.

[38] Reid Jr., J.B., Evans, O.C., Fates, D.G. 1983. Magma mixing in granitic rocks of the central Sierra Nevada, California. Earth Planet. *Sci. Lett.* 66, 243–261.

[39] Barbarin, B., Didier, J. 1991. Conclusions: enclaves and granite petrology. In: Didier, J., Barbarin, B. (Eds.), Enclaves and Granite Petrology. Elsevier, Amsterdam, pp. 545–549, ISBN: 0-444-89145-5.

[40] Barbarin, B. 2005. Mafic magmatic enclaves and mafic rocks associated with some granitoids of the central Sierra Nevada batholith, California: nature, origin, and relations with the hosts. *Lithos* 80, 155–177.

[41] Kemp, A.I.S., Wormald, R.J., Whitehouse, M.J., Price, R.C. 2005. Hf isotopes in zircon reveal contrasting sources and crystallization histories for alkaline to peralkaline granites of Temora, southeastern Australia. *Geology* 33, 797–800.

[42] Wang, K.X., Chen, P.R., Chen, W.F., Ling, H.F., Zhao, K.D., Yu, Z.Q. 2012.

 doi:10.20944/preprints201806.0344.v1

Magma mingling and chemical diffusion in the Taojiang granitoids in the Hunan Province, China: evidences from petrography, geochronology and geochemistry. *Mineral. Petrol.* 106, 243–264.

[43] Pearce ,J .A., Harris, N. B. W., Tindle A G.1984. Trace-element discrimination diagrams for the tectonic interpretation of granitic rocks. *J Petrol* 25, 956–983

[44] Bachelor, R.A., Bowden, P. 1985. Petrographic interpretation of granitoid rocks using multicationic parameters. *Chemical Geology* 48, 43–55.

[45] Demoux, A., Kröner, A., Liu, D.Y., Badarch, G. 2009. Precambrian crystalline basement in southern Mongolia as revealed by SHRIMP zircon dating. *International Journal of Earth Sciences* 98, 1365-1380.

[46] Li, Z.X., Bogdanova, S.V., Collins, A.S., Davidson, A., De Waele, B., Ernst, R.E., Fitzsimons, I.C.W., Fuck, R.A., Gladkochub, D.P., Jacobs, J. 2008. Assembly, configuration, and break-up history of Rodinia: a synthesis. *Precambrian Research* 160, 179-210.

[47] Lu, S.N., Li, H.K., Zhang, C.L., Niu, G.H. 2008. Geological and geochronological evidence for the Precambrian evolution of the Tarim Craton and surrounding continental fragments. *Precambrian Research* 160, 94-107.

[48] Shu, L.S., Deng, X.L., Zhu, W.B., Ma, D.S., Xiao, W.J. 2011. Precambrian tectonic evolution of the Tarim Block, NW China: New geochronological insights from the Quruqtagh domain. *Journal of Asian Earth Sciences Phanerozoic Continental Growth in Central Asia* 42, 774-790.